Cretaceous Research 100 (2019) 145–163

Contents lists available at ScienceDirect

Cretaceous Research

journal homepage: www.elsevier.com/locate/CretRes

A new faveoloolithid oogenus from the Wido Volcanics (Upper Cretaceous), South Korea and a new insight into the oofamily Faveoloolithidae

Noe-Heon Kim, Seung Choi, Seongyeong Kim, Yuong-Nam Lee*

School of Earth and Environmental Sciences, Seoul National University, Seoul, 08826, Republic of Korea

ARTICLE INFO

Article history:
Received 20 September 2018
Received in revised form
2 April 2019
Accepted in revised form 2 April 2019
Available online 9 April 2019

Keywords:
Dinosaur egg
Wido Volcanics
Faveoloolithidae
Secondary shell unit
EBSD
Epitaxy

ABSTRACT

The Cretaceous oofamily Faveoloolithidae has a unique shell unit and pore canal system that clearly differs from most of the extant and fossil eggshells. Despite its distinctiveness, morphological (micro- and ultrastructural) and crystallographic features of the Faveoloolithidae are poorly known. Here we report a new faveoloolithid nesting ground from the Upper Cretaceous siltstones within the Daeri Andesite of the Wido Volcanics (Coniacian–Santonian), South Korea. Forty-one of the same kind of dinosaur eggs distributed in at least eight clutches occur in seven different stratigraphic horizons, suggesting a colonial nesting ground and paleontological site fidelity (reuse of a site over geological time scale). These eggs were assigned to a new ootaxon, *Propagoolithus widoensis* oogen. et oosp. nov., based on a unique shell unit morphology which is branching towards the external part of eggshell, unlike other faveoloolithid eggs. New morphological and crystallographic features of *P. widoensis* provide a new insight into the oofamily Faveoloolithidae: (1) superimposed shell units, which are widely used as diagnoses of the Faveoloolithidae and Dictyoolithidae, are in fact taphonomic artifacts and (2) round and crystallographically upright shell units partially connected by inclined crystals (bridges) at the inner portion in the tangential section is proposed as an additional synapomorphy of the oofamily Faveoloolithidae. Furthermore, elemental analysis combined with light microscopy, EBSD, and CL analyses provide a successful reconstruction of the complex pore canal infilling process, and suggest that magnesium concentration can be used as a proxy for calcite overgrowth.

1. Introduction

Although four Asian oofamilies, namely the Dendroolithidae, Dictyoolithidae, Faveoloolithidae, and Similifaveoloolithidae (here we use the term the Dendroolithidae instead of the Phaceloolithidae, see S1 text) were first reported from China, Mongolia, and South Korea (Mikhailov, 1997a; Huh and Zelenitsky, 2002; Kim et al., 2011; Wang et al., 2011, 2012; He et al., 2017), recent discoveries and reassignment of faveoloolithid eggs from Uruguay and Argentina have extended their occurrence outside of Northeast Asia (Faccio, 1994; Grellet-Tinner and Fiorelli, 2010; Grellet-Tinner et al., 2012). These oofamilies are clearly distinguished from all other amniotic eggs by unique branching shell units and complicated pore canal system.

Due to complicated shell structure, however, parataxonomic confusions are frequent among these four oofamilies (Mikhailov, 1994, 1997a; He et al., 2017). Indeed, several ootaxa first assigned as one of these oofamilies (e.g., *"Dendroolithus shuangtangensis"*; *"Dendroolithus guoqingsiensis"*; *"Dictyoolithus gongzhulingensis"*) were misidentified, thereby their parataxonomic statuses have been revised (Jin et al., 2010; Zhang, 2010; Wang et al., 2011, 2013). Most of the previous studies on these eggs had focused on the description of general morphology from eggshell radial sections rather than understanding the three-dimensional eggshell structure, with the exception of micro-CT based study of Hechenleitner et al. (2016). Consequently, parataxonomic problems have been continuously perpetuated until today. Furthermore, mammilla-like secondary shell units observed at locations other than the base of eggshell, so-called superimposed shell units (*sensu* Zhao, 1994), are usually found in these four oofamilies. They are widely used as a

* Corresponding author.
E-mail addresses: thunderboy6@snu.ac.kr (N.-H. Kim), seung0521@snu.ac.kr (S. Choi), sykim2016@snu.ac.kr (S. Kim), ynlee@snu.ac.kr (Y.-N. Lee).

https://doi.org/10.1016/j.cretres.2019.04.001
0195-6671/

diagnostic character (Zhao, 1994; Zhang, 2010; Wang et al., 2011, 2013), although there is a high possibility that they are taphonomic artifacts rather than biological ones (Moreno-Azanza et al., 2016). In addition, the process or mechanism of eggshell formation has never been studied in detail for the Faveoloolithidae, despite their unique morphotype. Although Zhao (1994) proposed a tuatara model in which calcite crystals deposit simultaneously with shell membrane (Packard et al., 1988; but see also Cree et al., 1996) based on the presence of superimposed shell units, this model contrasts with the eggshell formation of archosaurs (Moreno-Azanza et al., 2013; Choi et al., 2018). In eggshells that have complex pore structure including the Faveoloolithidae, pores are commonly filled with a number of secondary calcite crystals (Vianey-Liaud et al., 1987; Huh and Zelenitsky, 2002; Grellet-Tinner et al., 2004) and even epitaxial crystals which have the same crystal orientation to that of neighboring shell units are observed (Grellet-Tinner et al., 2011; Moreno-Azanza et al., 2016). Nevertheless, this phenomenon has been little studied in eggshells.

Here we describe a new ootaxon of the Faveoloolithidae from a new dinosaur nesting ground found in the Upper Cretaceous siltstones of the Wido Volcanics, Wi Island, South Korea. This site produced forty-one *in situ* faveoloolithid eggs including eight clutches in seven different horizons. The purpose of this study is to provide a new comprehensive understanding of the oofamily Faveoloolithidae in regard to the parataxonomy, secondary shell unit genesis, three-dimensional microstructure, and nesting behavior with a suggestion that combined elemental and EBSD analysis can be used as a powerful method for reconstructing diagenetic process.

1.1. Institutional abbreviation

SNU, Seoul National University, Seoul, South Korea.

1.2. Technical abbreviations

CL, cathodoluminescence; PPL, plane-polarized light; XPL, crossed-polarized light; SEM, scanning electron microscope; BSE-COMPO, backscattered electron-composition; BSE-TOPO, backscattered electron-topography; EBSD, electron backscatter diffraction.

2. Geological setting

The Paleo-Pacific (Izanagi) Plate obliquely subducted beneath the Eurasian Plate during the Cretaceous, as a result, forming numerous NE-SW trending sinistral strike-slip fault systems with continental arc volcanism in the southern Korean Peninsula (Chun and Chough, 1992). A number of non-marine basins formed along the faults (Chough et al., 2000; Chough, 2013). Siliciclastic sediments intercalated with volcanic rocks filled the basins in the alluvial to lacustrine environment. The Wido Volcanics in Wi Island is one of the Cretaceous volcanic-sedimentary successions in the Korean Peninsula (Koh et al., 2013; Gihm and Hwang, 2014).

The Upper Cretaceous Wido Volcanics, located southwest of the Korean Peninsula, is composed of Daeri Andesite, Mangryeongbong Tuff, Beolgeumri Formation, and Ttandallae Tuff in ascending order (Fig. 1; Koh et al., 2013; Ko et al., 2017). The Daeri Andesite is made up of sedimentary rocks conformably overlain by andesite units (Koh et al., 2013; Gihm et al., 2017). The sedimentary rock, where numerous dinosaur eggs described in this study were found, is represented by 10 m thick reddish massive siliciclastic siltstones (Fig. 2A) with calcrete nodules interbedded with normal-graded medium to coarse sandstones (Fig. 2B). The siltstones interbedded with calcic horizons were interpreted as distal part of alluvial fan deposits developed in a semi-arid environment, while the sandstone was built by episodic debris flows (Bull, 1977; Blair and McPherson, 2009). Based on sandstones (Fig. 2B) and calcic horizons (Fig. 2C), seven different egg-bearing horizons were labeled (Fig. 2D). Two hundred fifty meters thick andesite unit covers the siltstones. The overlying Mangryeongbong Tuff consists of 600 m thick massive lapilli tuff, interpreted as pyroclastic density current deposits (Koh et al., 2013; Gihm and Hwang, 2014). U-Pb dating of zircon crystals indicates that the tuff was deposited 86.63 ± 0.83 million years ago (i.e., Coniacian–Santonian; Ko et al., 2017). Thus, the age of the egg-bearing deposit is older than early Santonian.

3. Material and methods

Forty-one *in situ* dinosaur eggs including eight clutches were discovered with hundreds of eggshell fragments from the reddish siltstones within the Daeri Andesite of the Wido Volcanics (Fig. 2A). A compressed incomplete egg (Figs. 3A–C) was collected from the outcrop as the holotype (SNUVP 201610). Two eggshell pieces (SNUVP 201701–201702) from half-breached eggs, one (SNUVP 201617) from the holotype, and ten isolated fragments (SNUVP 201301, SNUVP 201618–22, SNUVP 201703–06) were prepared for 30 μm thick radial thin sections with four 50 μm thick tangential thin sections (see S1 Fig. for the detailed location where tangential sections were made). Thin sections were examined under Nikon Eclipse LV100N polarizing microscope. Eggshell thickness was measured 244 times from twenty eggshell fragments using IMAGEJ v.1.48. SEM observation by JEOL JSM-7100F was carried out on SNUVP 201616 for studying eggshell ultrastructure using an accelerating voltage of 15.0 kV (School of Earth and Environmental Sciences, SNU). BSE-TOPO mode of SEM was used for SNUVP 201302 to identify eggshell surface ornamentation.

A chip for the radial thin section (SNUVP 201303; an eggshell fragment embedded in epoxy resin) and two tangential thin sections (SNUVP 201611 for the inner part of eggshell, SNUVP 201614 for the middle part of eggshell) were mechanically and chemically polished with 0.06 μm colloidal silica after polishing with 0.5 μm diamond pastes. For the description of the eggshell crystallographic architecture, EBSD analyses were performed on the prepared specimens using field emission SEM (JEOL JSM-7100F) fitted with an Oxford Instrument Symmetry detector (School of Earth and Environmental Sciences, SNU). AZtec software was used in automatically acquiring and indexing Kikuchi diffraction patterns. All obtained EBSD data of radial and tangential sections are provided as CPR and CRC Channel 5 files (S1 File). Wild spike (an isolated and wrong-indexed point) removal and low level zero solution (a non-indexed point) correction was performed to improve the quality of data. Zero solutions were removed by three times of extrapolation when it is surrounded by at least six adjacent pixels. The hit rate (fraction of successfully indexed pixels) improvement by wild spike removal and zero solution correction are as follows: Figs. 5A–B, 86.5 to 88.9%; Figs. 5C–D, 92.7 to 95.3%; Figs. 5E–F, 98.2 to 99.2%; Figs. 5G–H, 88.1 to 90.2%; Figs. 7A–B, 57.1 to 60.0%; Figs. 7C–D, 72.1 to 75.4%; Figs. 7E–F, 98.5 to 99.6%. Inverse pole figure (IPF) maps, grain boundary maps, Euler angle maps, and misorientation histograms were used to present the EBSD analyses. IPF-Y maps were used for radial sections of eggshell while IPF-Z maps were used for tangential sections to present the crystal orientation as the same color as IPF-Y maps. Therefore, in both the IPF maps, a crystal is presented in red color when its c-axis is perpendicular to the eggshell surface while in blue or green color when its c-axis is parallel to the eggshell surface. Misorientation angle (angular orientation difference between crystals) of 5°, 10°, and 20° were used as thresholds for grain boundary maps. Misorientation angle

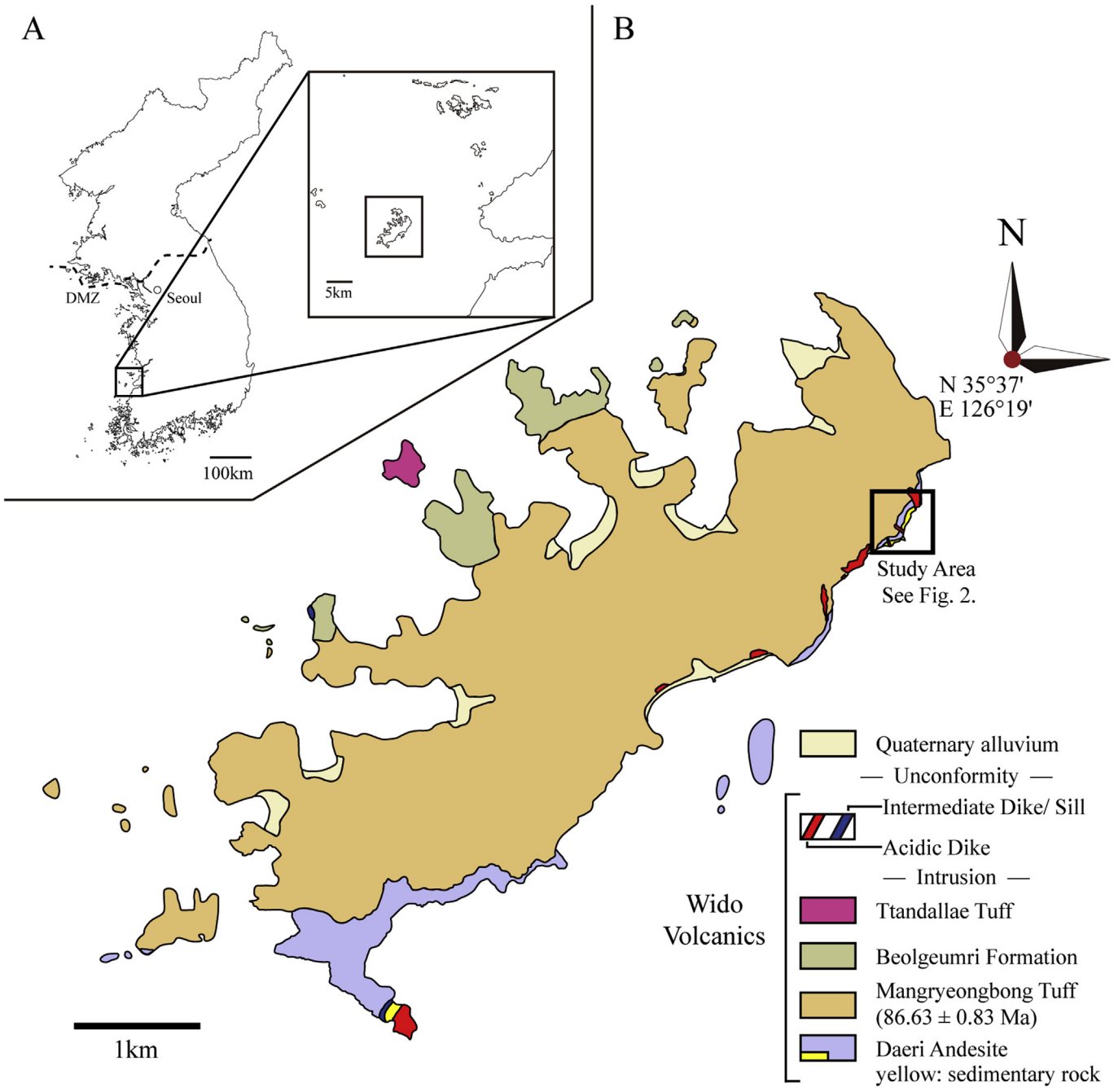

Fig. 1. Geological map of Wi Island. A. Geographical location of Wi Island in the southwest of the Korean Peninsula. B. The Wido Volcanics is composed of the Daeri Andesite, Mangryeongbong Tuff, Beolgeumri Formation, and Ttandallae Tuff. The Wi Island egg site marked by a square occurs in the coastal sedimentary outcrop on the east side of the Daeri Andesite. The egg-bearing deposit is no younger than 86.63 ± 0.83 Ma (i.e., Coniacian–Santonian) which is the radiometric age of the overlying Mangryeongbong Tuff (Ko et al., 2017) (modified from Koh et al., 2013; Ko et al., 2017). DMZ refers to Demilitarized Zone between South and North Korea. Color online. (For interpretation of the references to color in this figure legend, the reader is referred to the Web version of this article.)

lower than 5° was not used as such low angles are vulnerable to misorientation angle calculation (Prior, 1999; Sharma and Shekhar, 2018). Euler angle map is made by plotting three Euler angles with RGB colors, and this effectively shows the orientation of crystals. The step size of EBSD measurements are as follows: Figs. 5A–B, 3.5 μm; Figs. 5C–D, 0.7 μm; Figs. 5E–H, 0.6 μm; Figs. 7A–B, 2.2 μm; Figs. 7C–F, 2.5 μm.

Histograms of grain boundary misorientation angles of secondary shell units (both radially and transversally sectioned) and the inner portion of eggshell from *Propagoolithus widoensis* and *Megaloolithus* cf. *siruguei* were additionally made with neighbor-pair and random-pair distributions to quantitatively present the crystallographic nature of secondary shell units. EBSD data of *M.* cf. *siruguei* was retrieved from the supporting information of Moreno-Azanza et al. (2016). All areas where misorientation angle distributions were made are presented as S2 File as SUB Channel 5 files and S2 Fig. as an image file. Neighbor-pair misorientation distribution is made by misorientation calculation of adjacent grains while that of random-pair is made by calculation of randomly selected grains (Wheeler et al., 2001). The median, skewness, peak

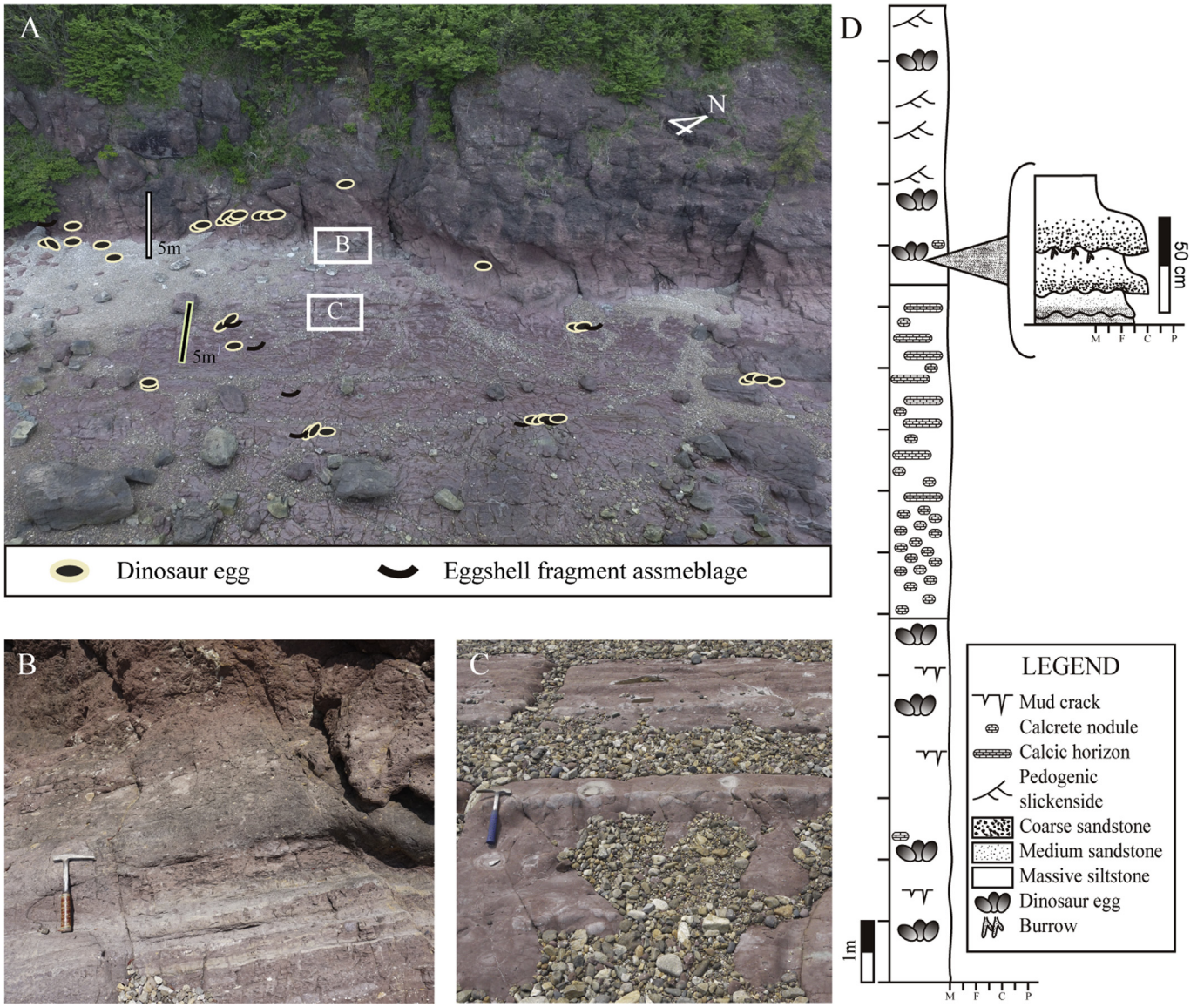

Fig. 2. Photographs of the Wi Island egg site. A. Aerial view of the egg site with dinosaur eggs and eggshells marked. Forty-one *in situ* dinosaur eggs including eight clutches were found from a vertical cliff and intertidal shore. B. An enlarged view of the sandstone layers interpreted as episodic debris flows. A hammer (37 cm long) for scale. C. An enlarged view of calcic horizons. A hammer (28 cm long) for scale. D. Columnar section of the Wi Island egg site. Seven different egg horizons occur in massive siltstones, implying multiple egg-laying events. Abbreviation: M, Mudstone (claystone and siltstone); F, Fine sandstone; C, Coarse sandstone; P, Pebble conglomerate. Color online. (For interpretation of the references to colour in this figure legend, the reader is referred to the Web version of this article.)

misorientation, proportion of misorientation below 20° of each distribution were further analyzed.

BSE-COMPO, cathodoluminescence (CL), and chemical analyses of nine elements were carried out on the same region of a radially sectioned chip (SNUVP 201303) where EBSD analysis was performed to estimate the extent of diagenesis and to trace the pore infilling history. All analyses were performed from FE-EPMA (JEOL JXA-8530F) housed in the National Center for Inter-University Research Facilities of SNU. BSE-COMPO mode of EPMA image was taken to examine the composition of pore canal infill. In BSE-COMPO image, heavy elements are shown as bright color while light elements as dark color.

A CL image was obtained to trace the diagenetic history particularly related to manganese (Grellet-Tinner et al., 2010). Manganese (Mn), the main cathodoluminescence inducer element, is often incorporated in pedogenic carbonate minerals, although the amount varies by fluid reduction-oxidation condition (Wilson and Evans, 2002), fluid composition (Barnaby and Rimstidt, 1989), and precipitation rate (Dromgoole and Walter, 1990) during calcite crystal formation. Therefore, the luminescence of CL image shows the secondary origin of calcite precipitation in eggshells, although quencher element such as iron should be considered. In contrast to optical, or “cold”, CL microscope which is widely used in petrology and paleontology (Grellet-Tinner et al., 2010; Ullmann and Korte, 2015), EPMA-CL, a scanning, or “hot”, CL method, was used in this study. Scanning CL has several advantages and limitations compared with optical CL method (Pagel et al., 2000). In optical CL, CL is produced by an electron gun attached to an optical microscope. It is useful in analyses of a large number of specimens since it does not require specimen coating and has a low price of stage. However, it has a low spatial resolution, thus unsuitable in high magnification, and also only provides qualitative results unless a CL

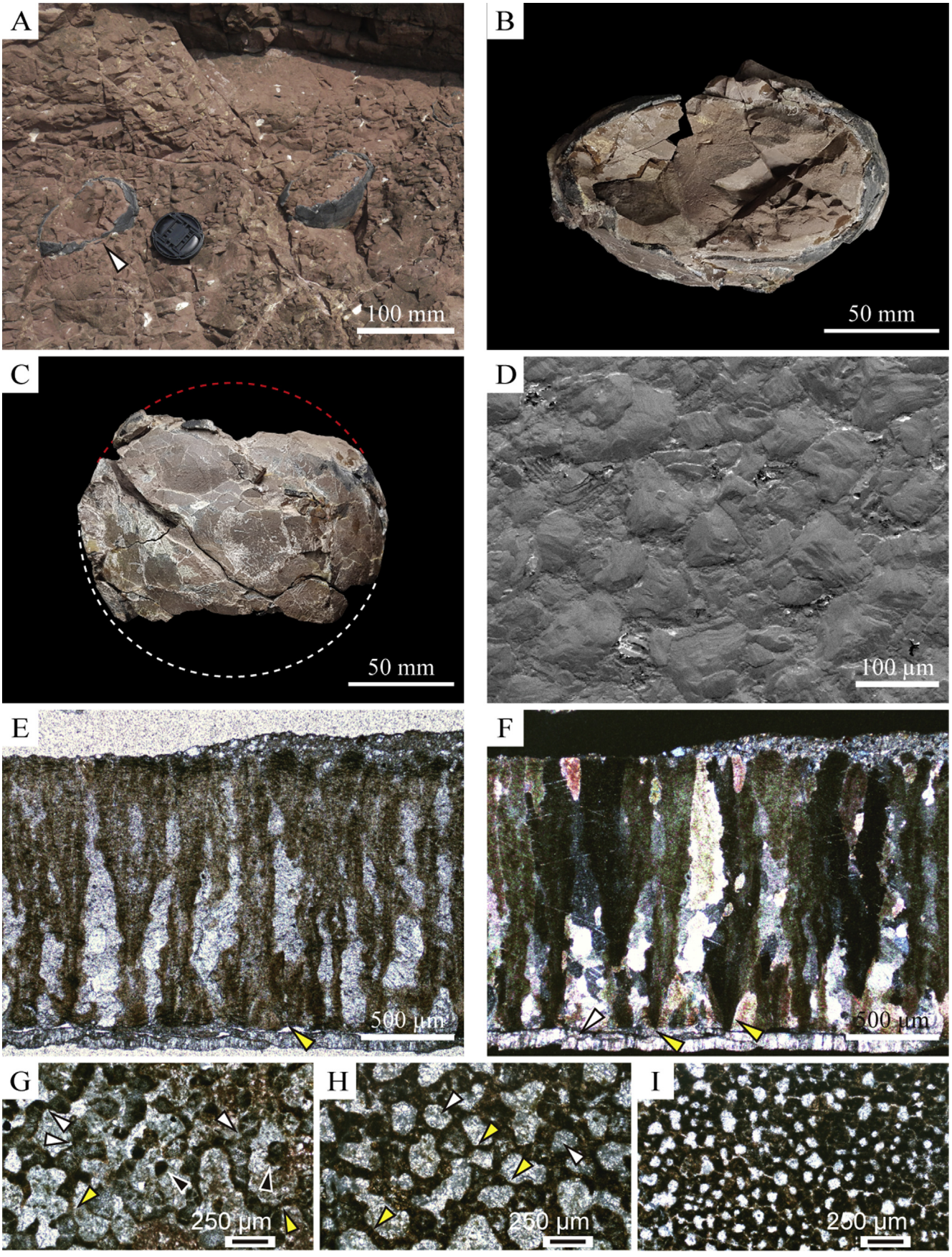
A
100 mm
B
50 mm
C
50 mm
D
100 μm
E
500 μm
F
500 μm
G
250 μm
H
250 μm
I
250 μm

spectrometer is additionally equipped. In contrast, EPMA-CL method has a high spatial resolution and provides precise and quantitative data which can be calibrated. Furthermore, since CL is part of an equipment of EPMA, it is also effective when coupled with BSE and elemental mapping by EPMA despite the requirement of specimen coating and high price of stage. Although this is the first attempt to use EPMA-CL in eggshells, scanning CL shares the same principle with optical CL and a number of studies in Earth Sciences which used scanning CL presented similar results with that of optical CL (Pagel et al., 2000 and references therein). Therefore, EPMA-CL image in this study is presented as red (high CL reactivity) in Mn-rich areas while as dark blue (low CL reactivity) in Mn poor or Fe rich areas, resembling the result of optical CL, but further providing an additional pseudo color bar as a quantitative data of CL reactivity.

The elemental mapping of nine elements (O, Na, Mg, Si, P, S, Ca, Mn, and Fe) was conducted. The purposes of examined elements are as follows: proxy for the sedimentary rock - O, Na, Mg, Si; proxy for the eggshell - Ca; trace elements incorporated in calcite that fills pore canals - Mg, Mn; elements known to exist in extant avian eggshells - Na, Mg, P, S (Pérez-Huerta and Dauphin, 2016; Dauphin et al., 2018); CL quencher element - Fe. The elemental mapping was conducted under accelerating voltage of 15.0 kV.

4. Systematic paleontology

Oofamily **Faveoloolithidae** Zhao and Ding 1976

Type oospecies. *Faveoloolithus ningxiaensis* Zhao and Ding, 1976; Cretaceous; Ningxia Province, China.
Revised diagnosis. Egg shape spherical to symmetrically spheroidal. Eggshell with (1) smooth or slightly nodular surface without ridges or conspicuously protruded nodes; (2) slender branching shell units; (3) irregular contour of pore canal margins in the tangential thin section near the inner surface; (4) numerous closely-spaced pore canals, forming a round honeycomb structure in the tangential thin section above the middle layer of eggshell.

Oogenus ***Propagoolithus*** oogen. nov.

Type oospecies. *Propagoolithus widoensis* oogen. et oosp. nov.
Etymology. Generic name from the Latin word *propago*, widen, for the shell unit widening towards the outer shell due to branching and from the Greek *oolithus* meaning stone egg.
Diagnosis. As for the type and only known oospecies.

Oospecies ***Propagoolithus widoensis*** oosp. nov.

Etymology. Species name from the Wido Volcanics where specimens were collected.
Holotype. SNUVP 201610, a compressed incomplete egg collected from the outcrop (Figs. 3A–C).
Referred specimens. A radial thin section (SNUVP 201301); Four tangential thin sections from an eggshell fragment (SNUVP 201611–14); Two mounted specimens for SEM observation (SNUVP 201302, 201616); A polished chip for EBSD and EPMA analyses (SNUVP 201303). All referred specimens are from isolated eggshell fragments.
Type locality. Siltstones within the Daeri Andesite of the Wido Volcanics of the northeastern Wi Island, Buan County, North Jeolla Province, South Korea.
Age. Late Cretaceous, older than 86.63 ± 0.83 Ma (i.e., older than Coniacian–Santonian; Ko et al., 2017).
Diagnosis. Faveoloolithid egg that has slightly nodulose surface and shell units branching out while pore canals accordingly gradually become smaller in diameter towards the outer eggshell.

Description.

In the outcrop, all eggs *in situ* including the holotype look as superficially ellipsoidal in shape (Fig. 3A). Most of the long axes of eggs are parallel to the bedding plane of the outcrop (Fig. 2A). However, the collected holotype (SNUVP 201610) is severely compressed (Figs. 3B, C), implying that the eggs were flattened along the stratigraphic horizon. This is not surprising since mudstone is strongly influenced by compaction (Nadon and Issler, 1997). Although some eggs are not aligned parallel to the main bedding plane, microfaults surrounding those eggs suggest that they were reoriented. Therefore, *P. widoensis* gives a good example for the importance of taphonomic effects on egg shape like other reports on distorted eggs affected by compression (Vila et al., 2010; Wilson et al., 2014; Hechenleitner et al., 2018). Although no complete clutch is exposed on the surface of the vertical outcrop, six closely positioned eggs in a horizon indicate that there was a minimum of six eggs in a clutch. Clutches occur in seven different stratigraphic horizons and some are juxtaposed within the same horizon, which imply colonial nesting and repeated use of the site of egg-layers in the context of geologic time scale. Most of the eggshells have a nodulose outer surface as clearly shown in BSE-TOPO image of SEM (Fig. 3D; SNUVP 201302), but some are smooth, possibly due to weathering (Clayburn et al., 2004). The average thickness of twenty eggshells is 1.62 mm (n = 244), ranging from 1.34 to 1.98 mm.

In a PPL image of the radial thin section (Fig. 3E; SNUVP 201301), the eggshell is composed of a single layer. Most of the shell units are slender (129 μm in average, ranging from 36 to 485 μm, n = 299; S3 Fig.) and branching out towards the outer eggshell (i.e., filispherulitic morphotype; *sensu* Mikhailov, 1997a). The surface of each shell unit is covered with a tiny node, making the eggshell surface nodulose. Slender shell units become wider towards the outer surface but some of them appear to be large by combining with neighboring shell units. Closely-spaced pore canals are well-developed and numerously distributed among irregularly branched shell units which are known as a diagnostic character of the multicanaliculate pore system. However, they are getting smaller and more abundant towards the outer eggshell surface, which is different from the uniform width of multicanaliculate pores presented in most faveoloolithid eggshells. In fact, it is more similar to prolatocanaliculate pore system (*sensu* Mikhailov, 1997a) in that pores vary in width along their height. Nevertheless, the

Fig. 3. Macro- and micro-features of *Propagoolithus widoensis* oogen. et oosp. nov. A. Two incomplete flattened eggs *in situ*. The egg with an arrowhead was excavated as the holotype (SNUVP 201610). B–C. Excavated egg as the holotype (holotype SNUVP 201610) in lateral and bottom views, respectively. White dot line indicates a damaged area while red one weathered one. D. BSE-TOPO mode of SEM showing the outer surface of eggshell (SNUVP 201302). Each of the tiny nodes corresponds to the uppermost surface of shell units shown in E–F. E. Radial thin section (SNUVP 201301) image under PPL. The eggshell is composed of a single layer. In general, shell units are widening and branching upwards while pore canals narrowing. If a connection between neighboring shell units is cut, shell units appear to be large (a yellow arrowhead). F. XPL image of (E). Note the undulose extinction of inner portion of shell units (yellow arrowheads). A fibrous secondary calcite layer occurs on the inner surface of eggshell (white arrowhead). G–I. Pore canal variations in tangential sections under PPL from the inner to the outer eggshell layer. G. Tangential thin section near the inner surface of eggshell (SNUVP 201611). Round-shaped shell units are easily observed (black arrowheads). Some of them are surrounded by irregular-shaped pore canals while others are connected by "bridges" (yellow arrowheads) or abutted to neighboring shell units (white arrowheads). H. A tangential thin section at the lower one-fourth of the eggshell (SNUVP 201612). Most of the shell units are continuously fused with each other (yellow arrowheads) between more isolated and rounded pore canals (white arrowheads) than the pore canals in (G). I. Tangential thin section at the upper one-fourth of the eggshell (SNUVP 201613). Well-separated pore canals make a honeycomb structure with tightly fused shell units. Pore canals are smaller and more rounded than those of inner layers. Color online. (For interpretation of the references to colour in this figure legend, the reader is referred to the Web version of this article.)

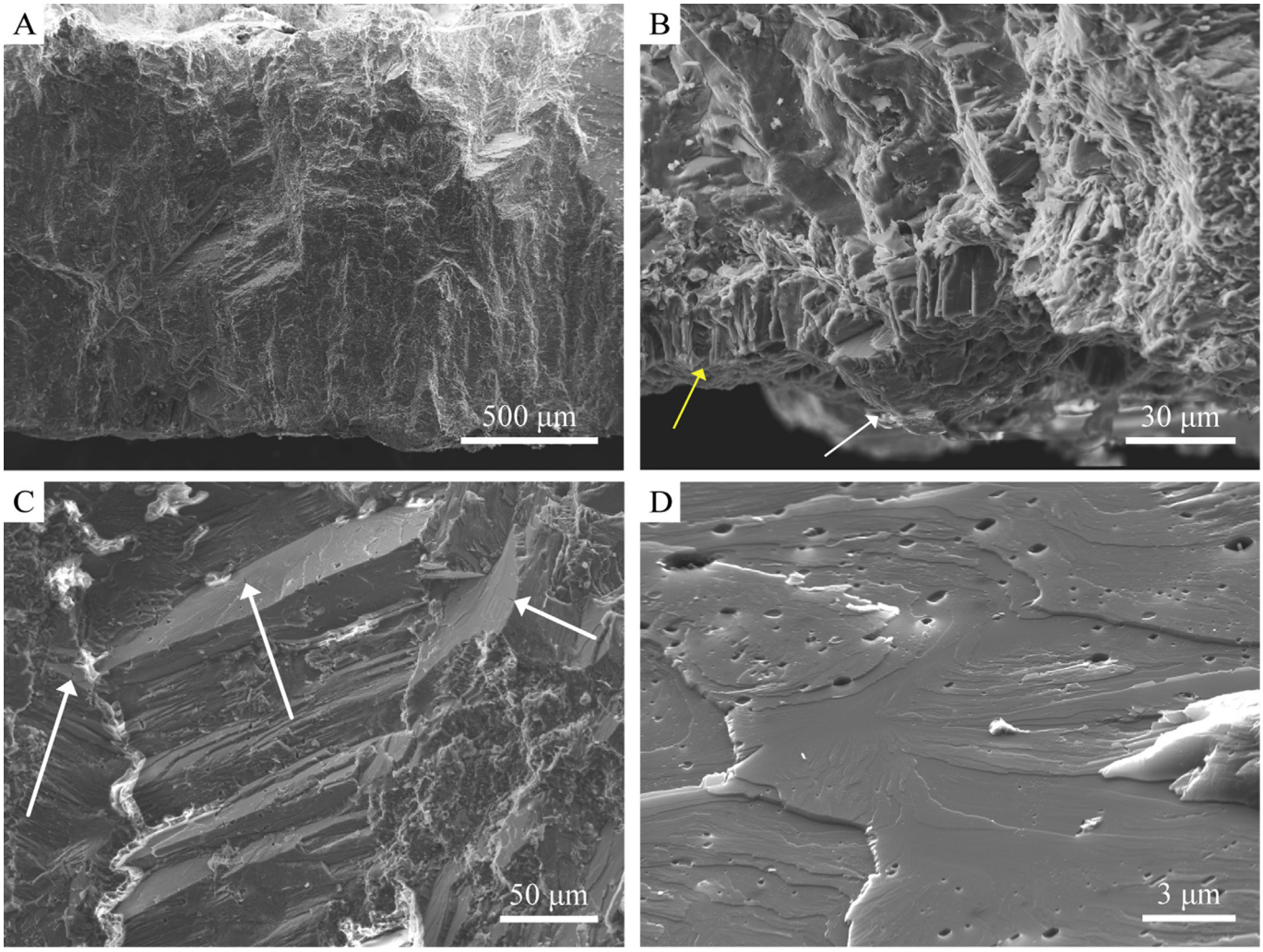

Fig. 4. Ultrastructural features of *Propagoolithus widoensis* oogen. et oosp. nov. by SEM (SNUVP 201616). A. Radial view of the eggshell. The eggshell is composed of a single layer. B. Ultrastructure of a lower portion of shell unit. A white arrow points to the base of a shell unit and the yellow arrow to the secondary fibrous deposit that is also shown in Figs. 3E, F. Radiating crystals that show tabular ultrastructure are observable in the inner portion of shell unit. C. Convergence of three prismatic columns (shell units) in the middle portion of eggshell. Columns that show tabular ultrastructure are aligned in different orientations (their growth directions are marked in arrows). D. Many different sized pits observed on the surface of a tabular crystal. The irregular shape and size imply taphonomic in origin. (For interpretation of the references to colour in this figure legend, the reader is referred to the Web version of this article.)

conical shape of pore canals clearly differs from irregularly shaped prolatocanaliculate pores. Therefore, it seems most reasonable to regard it as one of the variations of the multicanaliculate pore system. A XPL image shows a columnar extinction pattern of shell units (Fig. 3F). Although partly influenced by calcite dissolution and abrasion, the interior part of an eggshell is composed of small crystals which display undulose extinction (yellow arrows in Fig. 3F). However, the small crystals fuse to form a large crystal towards the external surface and each individual crystals shows discrete extinction. In general, numerous pore canals are filled with secondary calcites and/or siltstone.

In tangential thin section images, numerous pore canals are observable among complicatedly interconnected shell units. This is generally called a honeycomb structure which is found in all faveoloolithid eggs (Zhao, 1994; Zhang, 2010). However, shell units and pore canals vary dramatically in width and shape (Figs. 3G–I; see S1 Fig. for portions where tangential sections were made). Therefore, different types of the honeycomb structure are presented across the eggshell. First, numerous round-shaped shell units, resembling mammillary cones of multi-layered eggshells, are observable near the base of eggshell units (Fig. 3G; SNUVP 201611). Neighboring shell units are mostly abutted to each other while distant ones are connected with various shaped “bridges”. Large and irregular-shaped pore canals are surrounding rounded shell units and “bridges”. In a tangential section at the lower one-fourth of the eggshell (Fig. 3H; SNUVP 201612), most of the shell units are connected with each other but some are hemmed in between irregular to sub-circular pore canals (pore diameter: 217 μm in average, ranging from 85 to 388 μm, n = 100). The typical honeycomb structure of pore canals occurs at the upper one-fourth of the eggshell (SNUVP 201613) and pore canals are surrounded by tightly fused shell units (Fig. 3I). They are smaller and more round (92 μm in average, ranging from 55 to 166 μm, n = 100) than those of inner layers.

SEM observation of SNUVP 201616 reveals that the eggshell consists of a single structural layer which is made up of prismatic crystals (Fig. 4A). Despite the homogeneous ultrastructure presented throughout eggshell, gradual transition in orientation and size of crystals from the inner to outer portion is observed. Although calcite dissolution hampered the observation of the inner

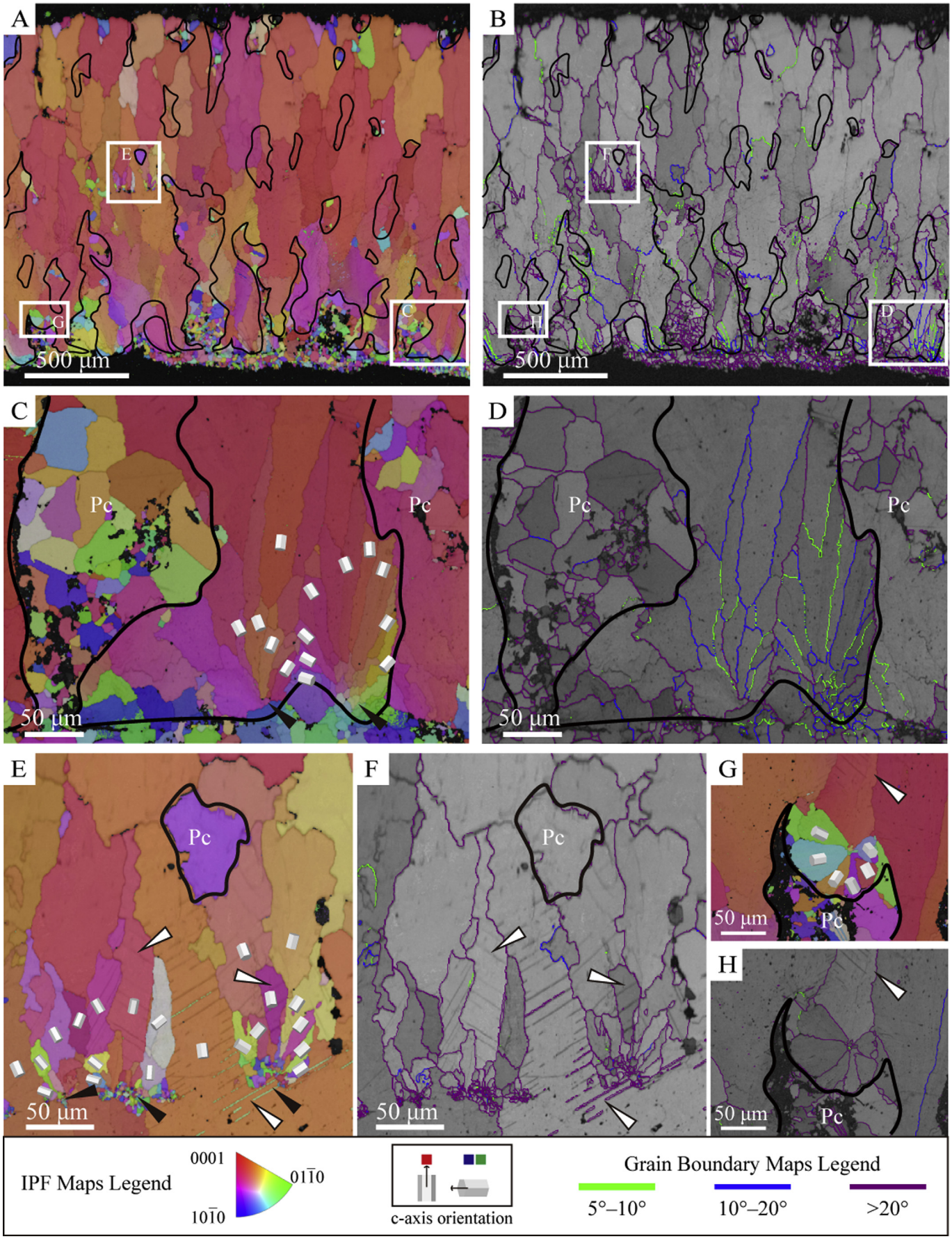
A
E
G
C
500 μm
B
F
H
D
500 μm
C
Pc
Pc
50 μm
D
Pc
Pc
50 μm
E
Pc
50 μm
F
Pc
50 μm
G
50 μm
Pc
H
50 μm
Pc
IPF Maps Legend
0001
01$\bar{1}$0
10$\bar{1}$0
c-axis orientation
Grain Boundary Maps Legend
5°–10°
10°–20°
>20°

portion of eggshell in most specimens, which is also reported in porous dictyoolithid eggshells (Jin et al., 2010), some well-preserved inner portions show small radiating crystals with tabular ultrastructure (white arrow in Fig. 4B). On the other hand, prismatic crystals of overlying columns are larger and more aligned towards the external surface, resembling stacks of paper (Fig. 4C). Each longitudinal columns corresponding to shell units grow in different spatial directions (white arrows in Fig. 4C). On the surface of tabular planes, numerous different sized pits, resembling vesicles or remnants of protein canals (Mikhailov, 1997a), are observed throughout the whole eggshell (Fig. 4D). However, the pits are more irregular in shape and size and also occur in the lower portion of eggshell unlike vesicles, implying their taphonomic origin.

Crystallographic studies by EBSD were performed both on the radial and tangential sections. IPF-Y maps and grain boundary maps are shown in radial section images (Fig. 5; SNUVP 201303). Outlines of pore canals are marked by black lines based on stereomicroscopic observation (see S4 Fig. for comparison between stereomicroscopic and EBSD image). In the radial section shown in the IPF map, most of the shell units are characterized by red to orange color (Fig. 5A). This indicates that the c-axis of calcite crystals is perpendicular to the eggshell surface. In contrast to well-aligned shell units, calcite crystals filled in pore canals near the inner and outer surface of eggshell are euhedral with a random c-axis orientation, which would appear as rhombohedric crystals in a SEM image (Grellet-Tinner, 2005, fig. 4A). Interestingly, most of the calcites in pore canals at the middle to outer portions are, however, composed of large upright crystals which have the same orientation with that of neighboring shell units. These crystals which retain the same crystal lattice of the attached substrate is called epitaxial crystals (Dickson, 1993). Accordingly, the grain boundary shown in EBSD (Fig. 5B), in many cases, does not coincide with the boundary of pore canal filled with epitaxial calcite as shown in a titanosaurian eggshell (Grellet-Tinner et al., 2011, fig. 3) and a megaloolithid eggshell (Moreno-Azanza et al., 2016). Shell units meet each other at high misorientation angles (orientation difference between crystals >20°) which are expressed by purple lines.

Besides radiation near the inner surface resembling the mammillary layer of multi-structural eggshells (Figs. 5C, D), the radiating crystals of the secondary shell units are observed at the middle and the lower portion of the eggshell (Figs. 5E–H). Superficially, they are very similar to true mammillae in morphology. However, there is a big difference in the degree of crystal radiation between them. Two abutting radiating crystals at the bases of the eggshell are composed of calcite crystals that show small orientation differences. Thus, they have low misorientation angles (5–20°) which are shown by a gradation of red to orange in the IPF map (Fig. 5C) and by green and blue lines in the grain boundary map (Fig. 5D). The low misorientation angle between crystals results in undulose extinction of the lower portion of eggshell in the radial thin section (Fig. 3F; Moreno-Azanza et al., 2013, 2017). As shown effectively in IPF and grain boundary maps, there is a gradual transition of crystal orientation and misorientation angle in the lower portion and overlying prismatic shell units.

On the other hand, three radial sections (Figs. 5E, F) and one transversal section (Figs. 5G, H) of the secondary shell units are composed of crystals having high misorientation angles (>20°), which are shown as discrete colors in the IPF maps and purple lines in the grain boundary maps (Figs. 5E–H). Furthermore, thin twinning is easily observed near and/or in the crystals of secondary shell units contrary to that of the inner portion of eggshell. Twin lamellae are perpendicular to c-axes of crystals composing secondary shell units. The radially sectioned secondary shell units in the middle portion of eggshell (Figs. 5E, F) are similar to those of superimposed shell units widely observed in the Faveoloolithidae, Dendroolithidae, and Similifaveoloolithidae (Zhang, 2010; Wang et al., 2011, 2013; Zhang et al., 2018) while a transversally sectioned secondary shell unit near the base of eggshell (Figs. 5G, H) resembles transversally sectioned extra spherulites of megaloolithid eggshells (Moreno-Azanza et al., 2016).

The distribution of misorientation angles between grains of the lower portion of eggshell and secondary shell units from *P. widoensis* and *Megaloolithus* cf. *siruguei* (Moreno-Azanza et al., 2016) are shown in histograms for further statistical comparisons (Fig. 6). Since the neighbor-pair misorientation better describes the crystallographic nature of adjoining crystals rather than random-pair misorientation, only neighbor-pair misorientation was used in the statistical calculation. *P. widoensis* shows a clear difference in misorientation distribution between the inner portion of eggshell and secondary shell units (Figs. 6A–C). The inner portion of an eggshell is characterized by the left-skewed histogram (skewness 1.8), which makes the low misorientation angle (<20°) account for 72.1% of total misorientation angles (Fig. 6A). Furthermore, the median and peak are formed at 13.3° and 10–11°, respectively. In contrast, both radial and transversal secondary shell units are skewed right (−0.1 and −0.7, respectively), indicating lack of low misorientation, which accounts for only 3.9 and 1.3%, respectively (Figs. 6B, C). In addition, the median and peak are also high (6B: 57.8°, 58–59°; 6C: 73.1°, 74–75°). In contrast to the distinct dichotomy of misorientation distribution in *P. widoensis*, however, *M.* cf. *siruguei* shows a much weaker difference in that of the eggshell inner portion and secondary shell unit (Figs. 6D–F). The inner portion of *M.* cf. *siruguei* also displays a left-skewed histogram (skewness 1.1), characterized by abundant low misorientation angles (median: 23.6°, peak: 6–7°; Fig. 6D). The portion of low misorientation (44.7%) is, however, much lower than that of *P. widoensis* (72.1%). Although the median (28.9°) and skewness (1.1) of radially sectioned secondary shell unit differ little from that of the inner portion, the peak of misorientation is formed much higher (34–35°), while the portion of low misorientation (23.3%) is nearly half of that of shell units (Fig. 6E). On the other hand, the misorientation distribution of transversally sectioned secondary shell unit shows a little difference in distribution and representative values from that of the lower portion of eggshell (Fig. 6F). The only noticeable difference is that the peak is formed in a higher misorientation (14–15°).

Two tangential sections near the inner surface (Figs. 7A–D) and one at the middle of the eggshell (Figs. 7E, F) are shown by IPF-Z maps and Euler angle maps. Two areas were analyzed in the

Fig. 5. Crystallographic features of the radial section of *Propagoolithus widoensis* oogen. et oosp. nov (SNUVP 201303). Boundaries of pore canals are marked by black lines based on stereomicroscopic observation. A, C, E, and G are IPF-Y maps while the others are grain boundary maps. A–B. Radial section of SNUVP 201303. Most of the shell units are crystallographically upright as shown in red to orange in the IPF map. Shell units meet each other with high misorientation (orientation difference between crystals) angle (>20°) which are expressed by purple lines in the grain boundary map. Pore canals are filled with many euhedral crystals at the inner and external portion of eggshell while being filled with big epitaxial crystals that share their orientation with adjoining shell units at the middle portion. C–D. Enlarged images of the inner portion of eggshell. It shows a gradation of red to orange in the IPF map and green or blue lines in the grain boundary map, implying upright but slightly differently oriented crystals. E–F. Enlarged images of three radially sectioned secondary shell units. G–H. Enlarged images of a transversally sectioned secondary shell unit. All of the secondary shell units in E–H exhibit discrete colors in IPF maps and purple lines in grain boundary maps. They indicate that the crystals are radiated in a wide range, having high misorientation angles. Note that thin twinning occurs in secondary shell units and/or their peripheries (white arrowheads). Abbreviation: Pc, Pore canal. (For interpretation of the references to colour in this figure legend, the reader is referred to the Web version of this article.)

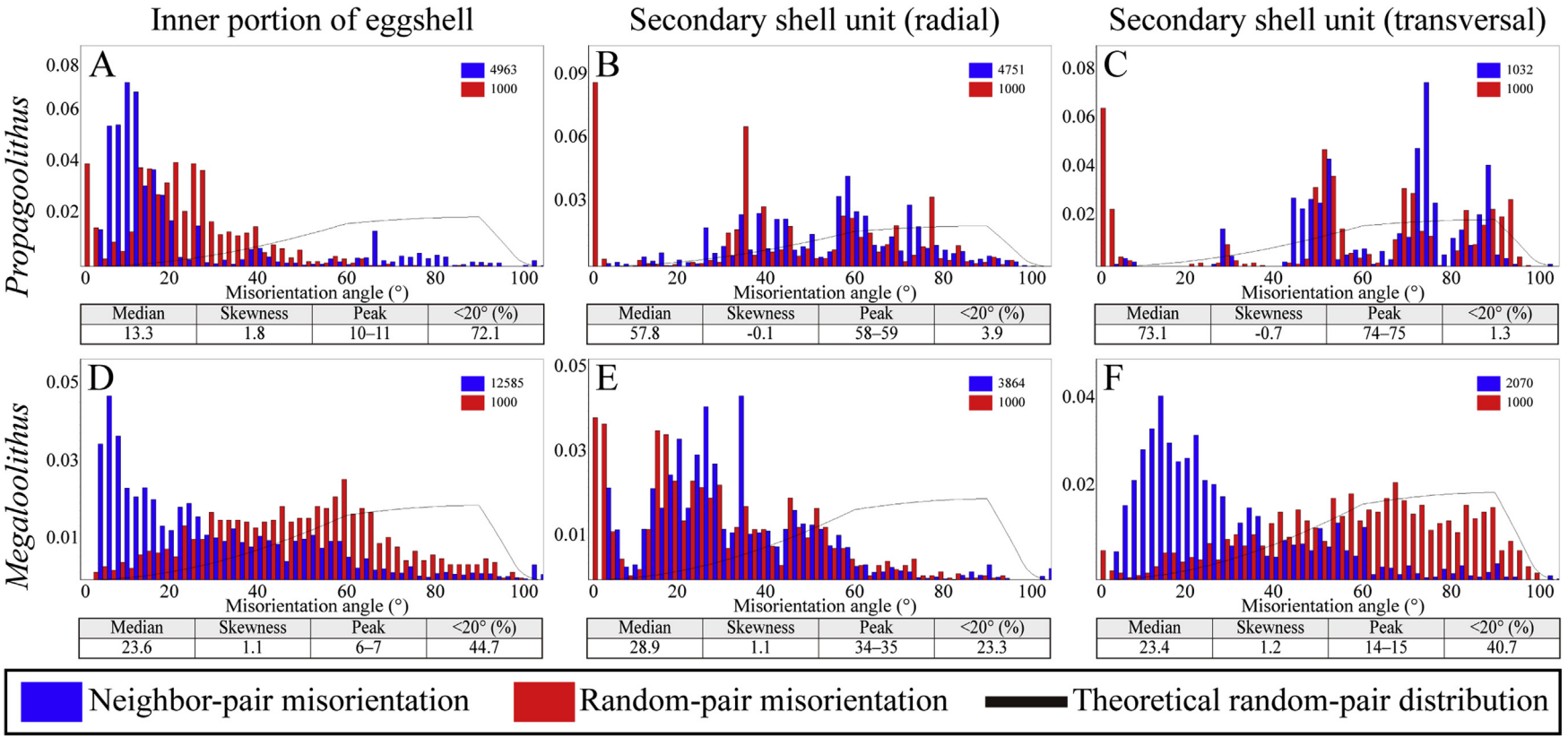

Fig. 6. Misorientation distribution of the inner portion of eggshell and secondary shell units from *Propagoolithus widoensis* oogen. et oosp. nov. and *Megaloolithus* cf. *siruguei* (from the supplementary data of Moreno-Azanza et al., 2016). The x- and y-axis represents misorientation angle and relative frequency, respectively. The blue columns are calculated under neighbor-pair method and the red columns under random-pair method. The black line represents theoretical frequency assuming random distribution. Values next to blue and red indices indicate measured sample size of each method. In *Propagoolithus* (A–C), the inner portion of eggshell (A) is characterized by low misorientation angles shown as a left-skewed histogram while secondary shell units (B, C) by high misorientation angles shown as a right-skewed histogram. In contrast, in *Megaloolithus* (D–F), the inner portion of the eggshell is also characterized by low misorientations but deviation between misorientations of secondary shell units (E, F) and that of the inner eggshell portion is much weaker than *Propagoolithus*. Color online. (For interpretation of the references to colour in this figure legend, the reader is referred to the Web version of this article.)

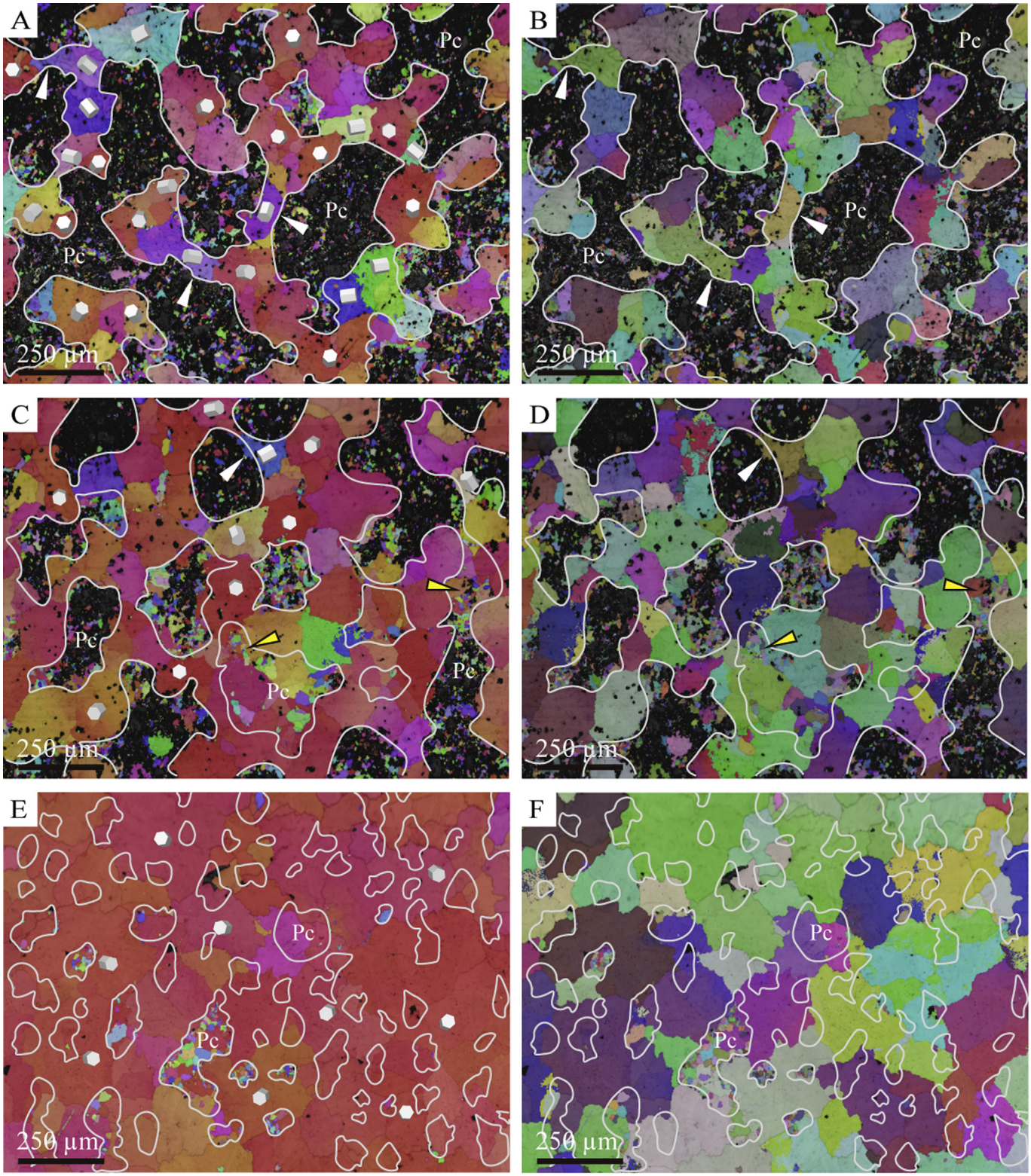

Fig. 7. Crystallographic features of tangential sections of *Propagoolithus widoensis* oogen. et oosp. nov. The boundaries of pore canals are marked by white lines in IPF-Z maps (A, C, E) and Euler angle maps (B, D, F) based on stereomicroscopic observation of the same region. A–B. Tangential sections near the inner surface (SNUVP 201611). Rounded shell units and their connections (i.e., bridges; arrowheads) form irregular outlines of pore canals. Crystals of the rounded shell units are upright (red) while bridges are inclined (blue or green). Euler angle map clearly shows different c-axis directions of shell unit crystals. Pores are filled with sedimentary infills and small euhedral calcite crystals. C–D. Marginal areas of the same thin section (SNUVP 201611), representing a slightly upper portion of eggshell due to eggshell curvature. Likewise, rounded shell units connected by bridges (white arrowheads) are observed. Pores are filled with larger euhedral crystals and some are surrounded by epitaxial crystals (yellow arrowheads). E–F. Tangential sections at the middle of the eggshell (SNUVP 201614). In contrast to the inner section (A–B), all crystals of the shell units are closely packed and upright (red). Some pore canals are filled with euhedral crystals but most of the infilled crystals present epitaxy. Therefore, boundaries between shell units and pore canals often do not coincide with crystallographic grain boundaries. Grain size as clearly shown in Euler angle map is larger than that of shell units in the inner section. Abbreviation: Pc, Pore canal. (For interpretation of the references to colour in this figure legend, the reader is referred to the Web version of this article.)

inner section (SNUVP 201611). On account of the curvature of eggshell, the central part of the thin section (Figs. 7A, B) represents a lower section of eggshell compared with the edge of the thin section (Figs. 7C, D). The irregular-shaped pore canals separated by round shell units and their connections (bridges) are observed (Figs. 7A–D) in both areas. With minor exceptions, most of the c-axes of shell units are upright (red) while bridges are inclined (blue or green) in IPF maps (Figs. 7A, C). This is quantitatively shown in the histogram of orientation difference between shell units and bridges (Fig. 8). Shell units have low orientation difference with the z-axis of eggshell (20.5° in median), thereby they are crystallographically upright. On the other hand, bridges have high orientation difference (54.6° in median), which means they are inclined. Euler angle map shows that bridges are composed of one to three grains oriented differently from adjoining shell units (Figs. 7B, D). At the middle section (SNUVP 201614), all crystals of the shell units are closely packed and separated by sub-circular pore canals (Figs. 7C, D). Unlike the binary orientation of shell units near the inner section, all of the shell units are oriented perpendicular to the eggshell surface as shown by red in IPF-Z map (Fig. 7C). Euler angle map shows that the shell units are tightly connected with different orientations (Fig. 7D). The grain size is larger than that near the inner section.

On the other hand, pore canal infill shows a compositional and crystallographic transition from the inner to middle portion of eggshell. The lowest portion is mostly filled with siltstone and a few euhedral calcite crystals (Figs. 7A, B), while a slightly upper section is filled with siltstone and euhedral crystals surrounded by epitaxial crystals attached to pore walls (Figs. 7C, D). The pore canal of the middle section is mostly composed of epitaxial crystals with some euhedral crystals, thereby in many cases, the boundaries of pore canals do not correspond to calcite grain boundaries. Therefore, it is impossible to detect pore canals filled with epitaxial crystals in the IPF map.

BSE-COMPO, cathodoluminescence (CL), and chemical analyses were performed on the radial section (SNUVP 201303) where EBSD analysis was done (Fig. 9). All shell unit-pore canal boundaries are drawn on the basis of stereomicroscopic observation (S4 Fig.). In BSE image, pore canals near the inner and outer eggshell surface were observed as bright (heavy element) calcite and dark (light element) sedimentary rocks, while pore canals at the middle to outer one-fourth portion did not show any difference with neighboring shell units (Fig. 9A). A magnified image of pore canals is characterized by various-sized pits also seen in Fig. 4D, indicating that the pits are probably taphonomic structures rather than vesicles. In a CL image (Fig. 9B), pore canals shown in bright color in BSE display strong CL signals (shown as yellow to orange color), while the unindexed pores in BSE show slightly stronger CL signals than neighboring shell units (white arrowhead) presented as light blue color. Furthermore, some small areas of the shell unit also show a strong CL signals, implying an alteration of some part of the shell unit (Fig. 9B, red arrowhead). Among the analyzed nine elements (S5 Fig.), four elements (Mn, Mg, Fe, and Si) were significant in revealing pore infilling history (Figs. 9C–F). Mn distribution is well

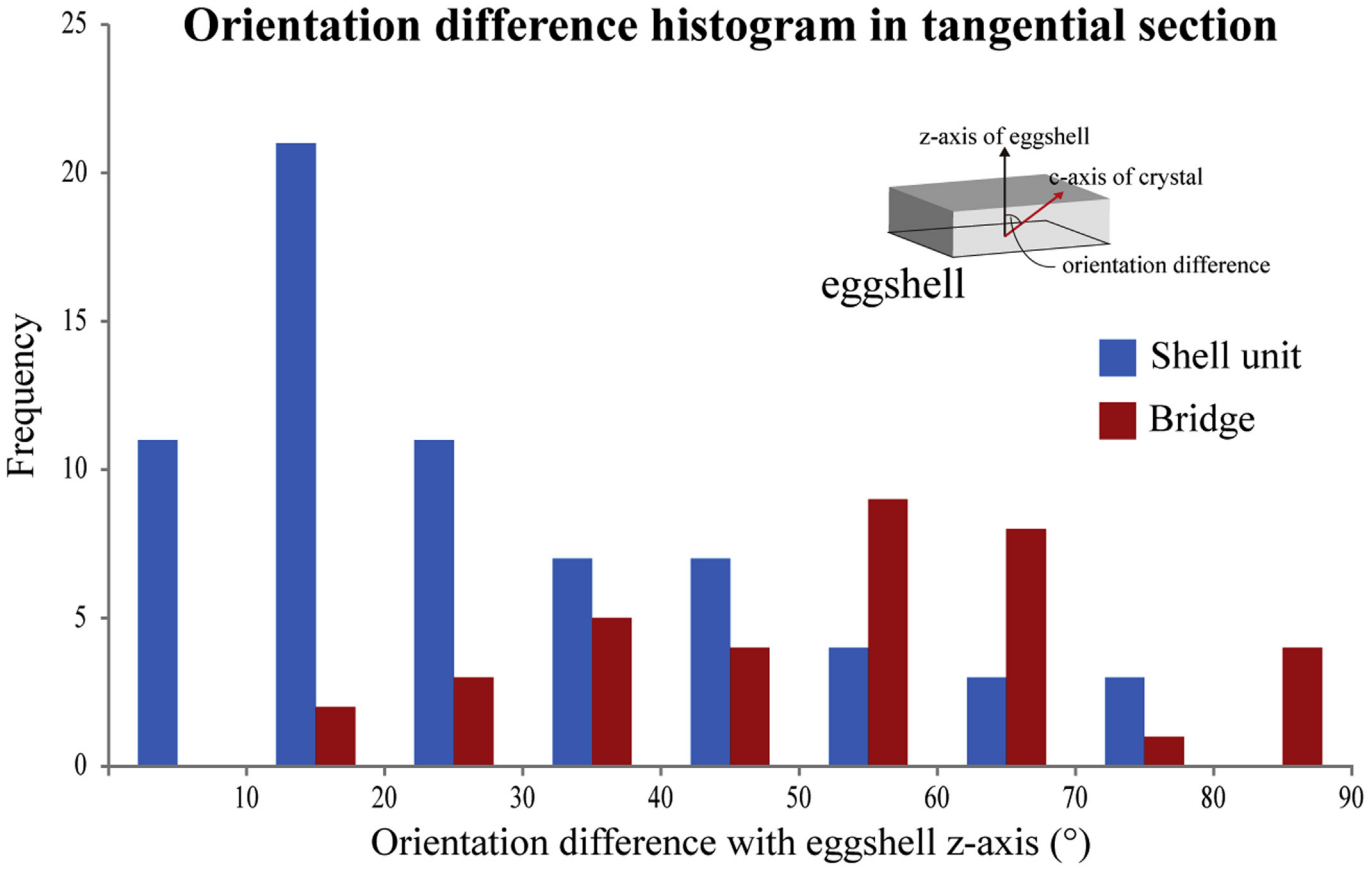

Fig. 8. Histogram of orientation difference of rounded shell unit and bridges in a tangential section of the inner eggshell (SNUVP 201611). Orientation difference between the z-axis of eggshell (axis perpendicular to the eggshell surface) was analyzed both on the rounded shell units (n = 67) and bridges (n = 36) in a tangential thin section using EBSD. Most of the mammillae have low orientation difference (20.5° in median), thus they are crystallographically upright. On the other hand, slender bridges that connect rounded shell units have relatively high orientation difference (54.6° in average). Color online. (For interpretation of the references to colour in this figure legend, the reader is referred to the Web version of this article.)

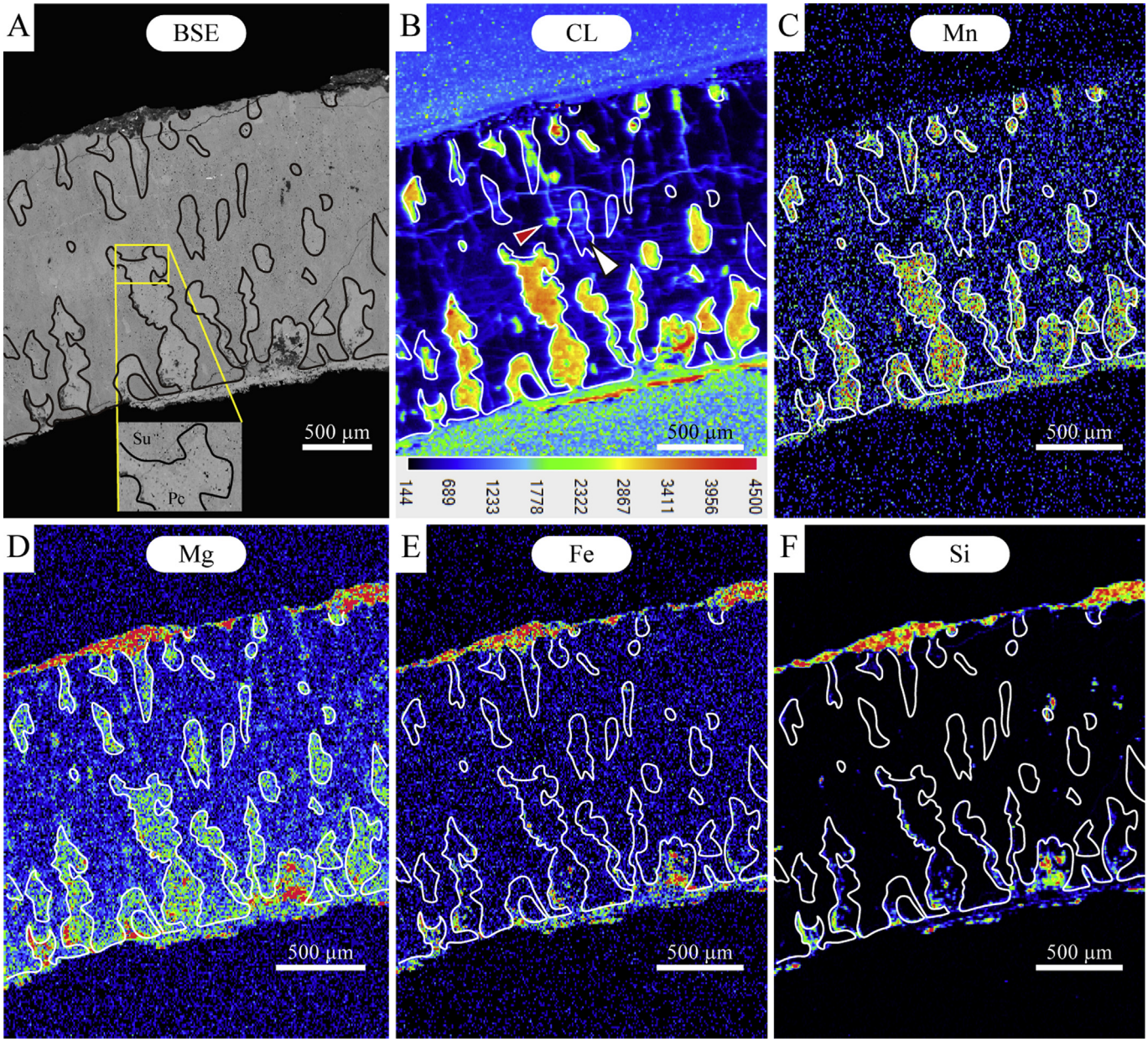

Fig. 9. Compositional distribution map of *Propagoolithus widoensis* oogen. et oosp. nov. (SNUVP 201303). A. BSE image. Pores near the inner and outer eggshell surface are brighter, indicating heavier elements. Magnified image shows that pits in Fig. 4D are also presented in calcite filling in pores, implying taphonomic in origin. B. CL image. Values below a pseudo-color bar represent relative intensities of CL. Beware that the relative intensity values are different from that of elemental maps (see S5 Fig.). Bright portions in BSE image present strong signal while pores undetected in BSE shows weak signal, as shown in light blue color (a white arrowhead). Some parts other than pore canals also present a strong signal (a red arrowhead), indicating the alteration of the shell unit. C. Mn map. Mn distribution coincides with the distribution of BSE and CL images. D. Mg map. Unlike BSE, CL, and Mn distribution images (A–C), the high concentration of Mg is observed in all pore canals. E. Fe map. Homogeneous signal presents throughout the eggshell, implying no quenching effect in CL signal. F. Si map. Sediments, shown effectively by Si, occur near the eggshell surface and boundaries of pore canals. (For interpretation of the references to colour in this figure legend, the reader is referred to the Web version of this article.)

matched with BSE image and areas of strong signal in a CL image (Fig. 9C). The minor deficiency of Ca (S5 Fig.) and dominance of heavy Mn of these pores indicate that the presence of $MnCO_3$ is a result of the substitution of Mn^{2+} for Ca^{2+} (Pingitore et al., 1988). In contrast to BSE and CL images, Mg distribution map presents all pore canals with strong signal (Fig. 9D). Mg-dominant calcites show greenish color while sedimentary rocks show red color. Fe and Si show that sedimentary infilling occurs near the inner and external surfaces of eggshell and boundaries of pore canals (Figs. 9E, F). The deficiency of Fe in eggshell implies that there are no quenching effects in CL. In secondary shell units, all nine elements do not show any signal that differs from neighboring shell units.

Detailed EBSD and EPMA analyses discriminated three types of pore infill based on epitaxy and Mg (Fig. 10). Type 1 characterized by Mn-depleted epitaxial crystal occurs in the middle to upper one-fourth portion. It is depleted in Mn, which show no or little signal in BSE and CL image (Figs. 9A, B). Type 2 that occurs closer to the eggshell surface than Type 1 is also composed of epitaxial crystals. However, Type 2 is Mn-rich shown as a strong signal in BSE and CL image (Figs. 9A, B) and slightly depleted in Ca (S5 Fig.) due to

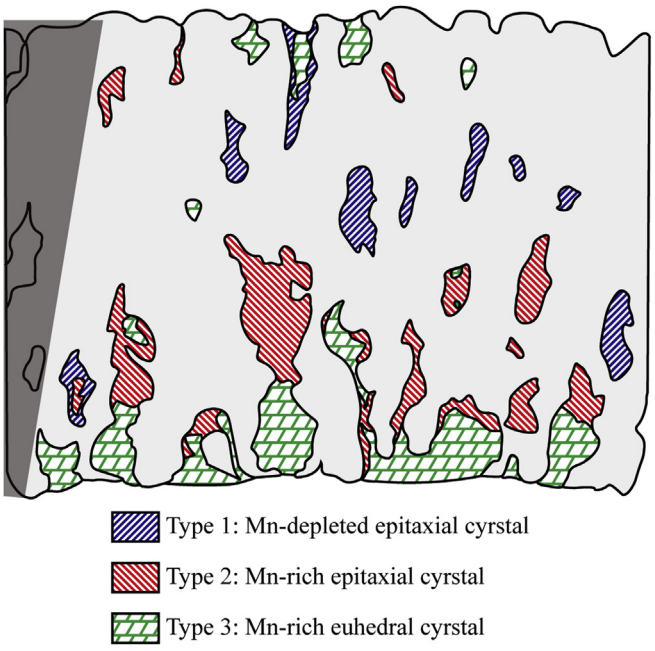

Fig. 10. Distribution of different pore-infilled calcite in the eggshell. Three types of pore infilling are identified based on epitaxy and Mn concentration. They are Mn-depleted epitaxial crystal, Mn-rich epitaxial crystal, Mn-rich euhedral crystal for Type 1 to 3, respectively. The shade indicates an unanalyzed area. Type 2 shares crystallographic nature with Type 1 while shares chemical composition with Type 3. Note that, in general, Type 1 to 3 appear successively from middle to inner/external surface, making a symmetry with respect to the middle portion of eggshell. Color online. (For interpretation of the references to colour in this figure legend, the reader is referred to the Web version of this article.)

substitution to Mn. Type 3 is observed near the eggshell surface which shares the same elemental distribution of Type 2, but it is composed of euhedral crystals. It is notable that the three types of pore infill show a symmetry with respect to the middle portion of eggshell. In other words, Type 1 to 3 occurs in sequence from the middle to inner/external portion.

5. Discussion

5.1. Parataxonomic assignment

Propagoolithus widoensis is composed of branching shell units and numerous pore canals, which are known as unique characteristics of the oofamilies Dendroolithidae, Dictyoolithidae, Faveoloolithidae, and Similifaveoloolithidae (He et al., 2017). Complicated shell units associated with numerous pore canals impede precise identification of each oofamily (Mikhailov, 1994, 1997a). Current diagnoses of the four oofamilies are parataxonomically incorrect in that (1) secondary shell units were used as a valid diagnosis, but they could be a taphonomic feature (Figs. 5E–H; Moreno-Azanza et al., 2016) and (2) important information on the three-dimensional eggshell structure was not included. Nevertheless, *P. widoensis* can be assigned to the oofamily Faveoloolithidae based on (1) long, slender, irregularly branching shell units (i.e., filispherulitic; *sensu* Mikhailov, 1997a); (2) closely-spaced long, narrow pore canals represented as the honeycomb structure in the tangential section (i.e., multicanaliculate; *sensu* Mikhailov, 1997a). The shell units of *P. widoensis* are much narrower than those of the Similifaveoloolithidae. Although the pore canals of *P. widoensis* change in width across the eggshell like those of the Dendroolithidae in radial sectional view, pore canals of the Dendroolithidae are very irregular, not like round pore canals of *P. widoensis*. Recently, eggs of *Torvosaurus* previously assigned to the Dendroolithidae were reassigned to the Faveoloolithidae (Zhang et al., 2018). Since pore canals of faveoloolithid eggs are much more round in the tangential section than that of *Torvosaurus* eggshell, however, the egg is likely to belong to a new oofamily. Due to many morphological variations in pore canals and shell units of the Dictyoolithidae, *P. widoensis* may look like a dictyoolithid egg, but the Dictyoolithidae has more slender shell units separated by denser and more irregular pore canals (Wang et al., 2013).

Five oogenera were assigned to the Faveoloolithidae: *Duovallumoolithus*, *Faveoloolithus*, *Parafaveoloolithus*, *Hemifaveoloolithus*, and *Youngoolithus*. Although the oofamily "Youngoolithidae" including the only oospecies *Youngoolithus xiaguanensis* was proposed (Zhang, 2010), we regarded it as invalid because there are no major differences between the Faveoloolithidae and "Youngoolithidae". The "Youngoolithidae" was mainly erected based on the ellipsoidal egg shape of *Y. xiaguanensis*, which differs from that of spherical faveoloolithid eggs. However, a single character cannot be used in parataxonomy since eggs exhibit great amount of homoplasy (Varricchio and Jackson, 2004). Furthermore, eggshell microstructure is consistent with the taxonomy of progenitor so that it can be used in parataxonomy (Mikhailov, 1997b). Although the microstructural difference between two oofamilies was pointed out that *Y. xiaguanensis* has irregular shell units (Zhang, 2010), they do not match with the long and straight shell units observable in thin sections of *Y. xiaguanensis* from Zhao (1979a) or Fang et al. (1998). On the other hand, the microstructure of *Y. xiaguanensis* is well matched with the main diagnosis of the Faveoloolithidae (i.e., slender branching shell units and numerous pore canals). Therefore, the "Youngoolithidae", erected on the basis of egg shape is probably a nomen dubium and *Y. xiaguanensis* should be reassigned to the Faveoloolithidae.

Shell units of *P. widoensis* branch out to the outer surface, so pore canals gradually become smaller (Figs. 3G–I). In contrast, there are no significant changes in the shell unit and pore canal width in other faveoloolithid oogenera (i.e., *Duovallumoolithus*, *Faveoloolithus*, *Parafaveoloolithus*, and *Youngoolithus*) with an exception of *Hemifaveoloolithus* (Fig. 11). In *Hemifaveoloothus*, however, the decrease in pore canal width towards the external eggshell surface is significantly more abrupt than *Propagoolithus*, resulting in a low density of pore canals above the middle portion (Wang et al., 2011). Moreover, *P. widoensis* (shell unit range: 36–485 μm, average: 129 μm; S3 Fig.) has thicker shell units than those of *Parafaveoloolithus* (shell unit range: 23–130 μm, average: 85 μm; Zhang, 2010, fig. 4). Faveoloolithid eggs were also reported from Argentina and Uruguay (Faccio, 1994; Grellet-Tinner et al., 2012). However, their thick eggshell which exceeds 4 mm (Grellet-Tinner et al., 2012) and shell unit composed of acicular crystals (Grellet-Tinner and Fiorelli, 2010) cast doubt on its assignment to the Faveoloolithidae. Thus, *P. widoensis* differs from all known faveoloolithid eggs in the morphology of the shell unit and pore canal pattern.

5.2. Taphonomic origin of the secondary shell unit and its implications to ootaxonomy

The secondary shell unit is frequently observed in a wide range of fossil oofamilies by three different types: (1) double-layer type, secondary shell units start above ordinary shell units in a uniform height within eggshell (Jackson and Schmitt, 2008); (2) extra spherulite type, tiny and oblique shell units appear in different heights in the eggshell (Moreno-Azanza et al., 2016); (3) superimposed shell unit type, normal sized and upright shell units are observed in different height within the eggshell (Zhao, 1994). Among them, the superimposed shell unit (type 3) is the most

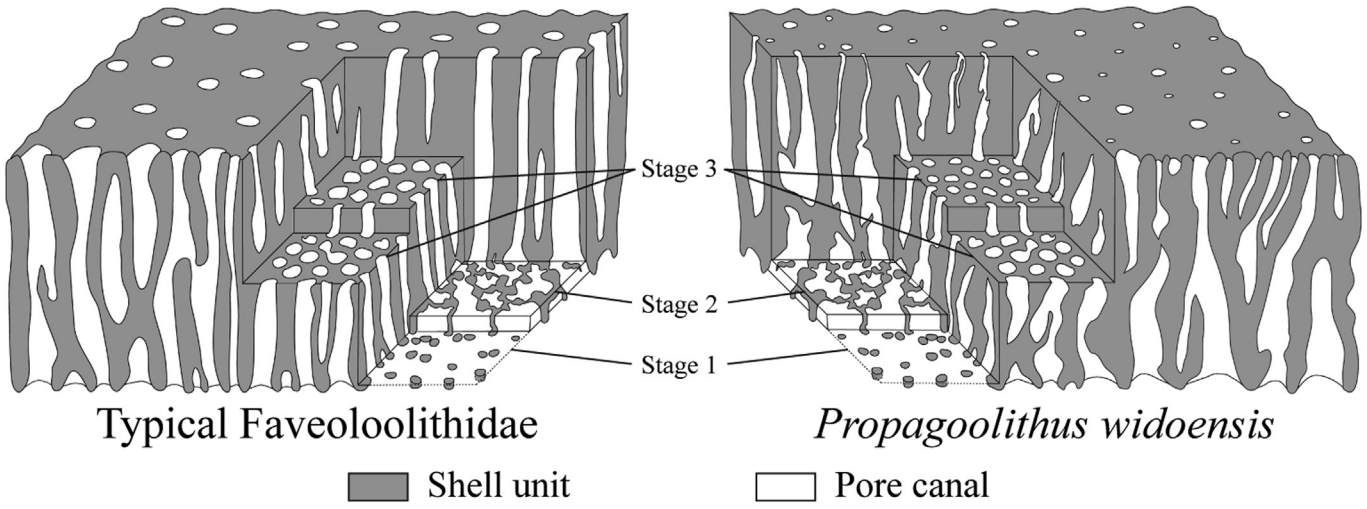

Fig. 11. Shell formation of typical Faveoloolithidae and *Propagoolithus widoensis* oogen. et oosp. nov. Gray color for shell units and white for pore canals. The surface ornamentation of eggshell was omitted to show the pattern of pore canals. Stage 1, crystals are radiating upwards from organic cores of the inner portion of eggshell. Stage 2, some rounded shell units connected to neighboring shell units by bridges form irregular outlines of pore canals. Stage 3, all of the shell units are fully connected to each other except for sub-rounded to rounded pore canals, forming a honeycomb structure. Note that pores become rounder as they are closer to the outer surface of the eggshell. Typical faveoloolithid eggshells retain pore canal widths but the pore canals of *P. widoensis* decrease in size towards the outer surface due to shell units branching upward. The typical faveoloolithid structure was drawn based on thin section images in Zhang (2010).

common phenomenon in the oofamilies Faveoloolithidae (Zhang, 2010; Zou et al., 2013), Similifaveoloolithidae (Wang et al., 2011), Dendroolithidae (Zhang et al., 2018), and Dictyoolithidae (Zhao, 1994; Liu and Zhao, 2004; Kim et al., 2011; Wang et al., 2013). It is widely used as a diagnostic character in parataxonomy and even new oogenera within the Dictyoolithidae, namely *Paradictyoolithus* and *Protodictyoolithus*, which were erected based on the number of superimposed shell units (Wang et al., 2013). Furthermore, Zhao (1994) hypothesized that superimposed shell units were formed by repeated processes of simultaneous eggshell calcification and shell membrane formation, resembling the eggshell formation of tuatara (Lepidosauria) suggested from Packard et al. (1988). Since this differs from the general mechanism of eggshell formation in the Archosauria, he regarded superimposed shell units as an evolutionary trait.

However, our EBSD study on *P. widoensis* supports a taphonomic origin of superimposed shell units rather than a biological trait. The misorientation angles among calcite grains of a secondary shell unit are much larger (>20°) than those of the inner portion of eggshell (<20°) (Figs. 5, 6A–C). Moreover, thin twinning occurs near and/or in the crystals of a secondary shell unit, unlike the inner portion of eggshell. As thin calcite twinning (known as e-twinning) is a common result of recrystallization under strain with low temperature (Ferrill et al., 2004), secondary shell units could be diagenetic in origin. Furthermore, it has been observed that thin twinning can be presented on eggshell by mechanical stress (Schmidt, 1962; Tyler and Moore, 1965). Interestingly, twinning lamellae occurred in secondary shell units are perpendicular to c-axes of crystals composing them (Fig. 5F). It is known that thin calcite twin lamellae are formed perpendicular to the compression direction (Groshong, 1972). This implies that the paleostress orientation of each crystal in a secondary shell unit is parallel to its c-axis. Simple external forces exerted on the eggshell are difficult to explain the radiating paleostress orientations of crystals composing a secondary shell unit. Therefore, we hypothesize that thin twinning inside the grain boundaries of a secondary shell unit was made when the secondary shell unit grew up to push the overlying shell unit. This mechanism might explain why there is mechanical twinning in a superimposed shell unit (Fig. 5F), but no extra-spherulites. They grow obliquely to the eggshell growth direction, and thereby unlikely to experience stress during growth as there are no overlying shell units to push (Moreno-Azanza et al., 2016, fig. 6B). It is noteworthy that many dictyoolithid eggshells having superimposed shell units often show calcite twinning (Kim et al., 2011, fig. 6C; Wang et al., 2013, figs. 1, 5). Interestingly, superimposed shell units occur mainly in the morphologically similar oofamilies such as the Faveoloolithidae and Dictyoolithidae. If all superimposed shell units are taphonomic phenomena in these ootaxa, this trait could be related to a unique and complicated pore canal system. Pore canals or interspace between shell units are vulnerable to be altered with an external fluid (Graf et al., 2018). In fact, taphonomic extra spherulites, a type of secondary shell unit, were recently reported near the pore canals in megaloolithid eggs (Moreno-Azanza et al., 2016). Therefore, it is reasonable to postulate that the secondary shell unit is closely related to highly porous eggshells. However, it is uncertain that secondary shell units are made by external fluid. At least the nine elements in this study failed to show any compositional difference with neighboring shell units but showed a compositional difference with pore infilled calcite (Fig. 9; S5 Fig.). Although an association of external fluid with a secondary shell cannot still be ruled out, this might imply that the resource that makes a secondary shell unit came from neighboring shell units rather than external fluid itself. Further crystallographic and chemical research is needed to understand the exact genesis of a secondary shell unit related to mechanical stress and pore fluid.

Our study is concordant with a notion of Jin et al. (2010) that the superimposed shell unit is not a true mammilla because of the absence of nuclei. Although we are not arguing that all superimposed shell units were diagenetically altered, a taphonomic or crystallographic analysis should be carried out to the alleged secondary shell units before the parataxonomic assignment or taking them as an evolutionary trait, especially in porous eggshells. Therefore, new ootaxonomic investigations are necessary for many oogenera that are highly porous. For instance, if the secondary shell unit used as a main diagnostic character of *Paradictyoolithus* and *Protodictyoolithus* turns out to be a taphonomic feature, the

parataxonomy of the Dictyoolithidae should be heavily revised. Thus, EBSD analysis can be used as a powerful tool to detect diagenetic features such as secondary shell units in fossil eggshells (Moreno-Azanza et al., 2016).

5.3. Three-dimensional microstructure of the Faveoloolithidae

The Faveoloolithidae is characterized by the complicated shell unit with a unique pore canal structure. For instance, the honeycomb structure with round pores observable in tangential sections (Figs. 3G–I) does not exist in any extant and fossil amniotic eggs. Despite its distinctiveness, the process of shell formation is poorly known. A hypothesis of tuatara-like eggshell formation was proposed by Zhao (1994) based on the superimposed shell units but it is rejected here as discussed above. EBSD analyses on both radial and tangential sections allow us to reconstruct the process of faveoloolithid eggshell formation.

It has been proposed that faveoloolithid eggshells are monolayered and shell units should not be subdivided into the mammilla and upper part of eggshell (Mikhailov, 1997a; Grellet-Tinner and Fiorelli, 2010). Nevertheless, XPL, SEM and EBSD images in *P. widoensis* (Figs. 3F, 4, 5A–D) show that the lower portion is composed of radially oriented small crystals while the overlying portion is composed of upright and large crystals. However, this should not be taken into account in describing structural layers of eggshell since the transition of crystal orientation and size is observed in all dinosaurian eggshells (Moreno-Azanza et al., 2013). For instance, spheroolithid eggshells from Tiantai basin have been misinterpreted as having two structural layers, but the same micro- and ultrastructure presented throughout the eggshell revealed that they were composed of a single layer (Barta et al., 2014). Furthermore, the gradual structural transition of prismatic crystals resembles that of the multi-layered Prismatoolithidae. However, unlike the prismatoolithid transition from tabular to squamatic ultrastructure, *P. widoensis* solely presents tabular ultrastructure in SEM. The absence of rugged grain boundaries in shell units further supports the absence of squamatic ultrastructure (Choi et al., in press). Therefore, the homogeneous tabular ultrastructure presented both in the inner and overlying portion of *P. widoensis* indicates faveoloolithid eggshells are mono-layered. The Dictyoolithidae also has tabular but non-squamatic shell units (Jin et al., 2010) with a single layer.

In this paper, we divide the eggshell structure of Faveoloolithidae into three different morphologies in the three-dimensional sections (Fig. 11). At stage 1, numerous small shell units are observed (black arrows in Fig. 3G). Their crystals radiate upwards like other dinosaurian eggshells (Figs. 5C, D; Moreno-Azanza et al., 2013). At stage 2, radiating crystals of shell units start to meet with neighboring shell units (Fig. 3G). Although a few shell units retain their original rounded shape, most of them connect to each other by variously shaped bridges, making irregular outlines of shell units in cross section. Consequently, outlines of the pore canals are irregular as well. These shell units are made up of upright crystals but crystals of bridges have inclined c-axes (Figs. 7A, B; Fig. 8). Bridges are made up of one to three crystals that meet neighboring radiating shell units with high misorientation, implying that new crystals grew to form bridges that connected neighboring shell units. This unique connecting system of shell units seems to be related to making a unique honeycomb structure of the Faveoloolithidae. In contrast to the compact prismatic layer of avian eggshells formed by the convergence of cone-shaped mammillae (Dalbeck and Cusack, 2006), faveoloolithid eggs have a well-developed porous system above the inner portion of eggshell. Therefore, shell units in the inner portion of Faveoloolithidae do not converge completely but connect to each other by bridges, leaving wide open space for pore canals. Stages 1 and 2 occur at the innermost part of eggshell, indicating a fast transition between the two stages. Hence, a mixture of the two stages is easily observed in the innermost tangential sectional view (Fig. 3G). At stage 3, all of the shell units are closely packed but only separated by sub-rounded to rounded pore canals, forming a honeycomb structure (Figs. 3H, I). The inner part of stage 3 shows two or three connected pore canals (Fig. 3H). However, as pore canals become closer to the outer surface, they are more isolated and rounded (Fig. 3I). In contrast to stage 2, all c-axes of shell units are perpendicular to the eggshell surface (Figs. 7E, F).

The complex eggshell structure sometimes causes mistakes in ootaxonomy because different shell unit morphologies in radial sections may appear even in a single eggshell (Mikhailov, 1997a). In that sense, it is important for ootaxonomic identification to understand the three-dimensional microstructure of Faveoloolithidae. One of the frequently used characters to distinguish the Faveoloolithidae from others is the honeycomb structure found in tangential sections (Stage 3 in Fig. 11; Mikhailov, 1994). Therefore, it is necessary for correct identification and classification of Faveoloolithidae to understand how the honeycomb structure was constructed. As Zhao (1979b) and Zhang (2010) mentioned, the proper honeycomb structure does not appear near the inner surface of eggshell (Stage 2 in Fig. 11) because pore canals are irregularly connected to each other, partially surrounding shell units. This morphology of tangential section corresponding to the inner portion of eggshell was already reported in all oogenera of the Faveoloolithidae (Zhang, 2010) including *P. widoensis* except for *Hemifaveoloolithus* whose inner tangential section was not made (Wang et al., 2011). Therefore, rounded shell units and their connections separated by irregular pore canals shown in the inner portion of eggshell can be a diagnosis of the oofamily Faveoloolithidae. The shell unit width is also of importance in ootaxonomic ranks, maybe oogenus or even oofamily levels. The exact shell unit width can be measured from 3D reconstruction images by micro-CT scans (Araújo et al., 2013). However, when it is not available, we need to take enough measurements to obtain statistically significant numbers from radial sections because they can be changed significantly by the cutting angle of the honeycomb structure (arrow in Fig. 3E; S3 Fig.).

5.4. Pore infilling process and its implication of epitaxial overgrowth to eggshell studies

Calcite crystals filling pore canals in *P. widoensis* fall into three types (Fig. 10). The composition of Mn and Fe gives a clue in revealing pore infilling events. Both Type 1 and Type 2 infills are epitaxial, therefore are indistinguishable in an EBSD image (Fig. 5A). However, their Mn composition is greatly different from each other, showing a sharp boundary of distribution (Fig. 9). Mn composition in calcite may differ even when precipitated from the same fluid under different precipitation rate (Dromgoole and Walter, 1990) and redox environment (Barnaby and Rimstidt, 1989). However, this process also brings a difference in Fe composition at the same time. The absence of any distributional difference of Fe in pores indicates that Type 1 and Type 2 infills were made by different pore infilling events rather than the evolution of the same fluid. Therefore, the difference in Mn composition is due to different Mn concentration of the pore infilling fluids. In contrast to the crystallographic continuity but the elemental discontinuity between Type 1 and 2, it is reverse between Type 2 and 3 (Fig. 10). The subtle deficiency in Ca and abundance in Mn (S5 Fig.) implies that substitution of Mn^{2+} for Ca^{2+} occurred in the pore fluid (Pingitore et al., 1988). Since Type 2 and 3 show homogeneous elemental distribution, it is unclear they were made by same pore infilling event or by different fluids which show similar

composition. Observation and analyses of several thin sections (Figs. 3G–I, 7A–F, 9; authors' pers. obs.) show that the sedimentary rock in pores is always presented near the inner and outer surface and/or boundaries of pore canals, while calcite is presented at the middle portion of eggshell. Furthermore, a symmetry with respect to the middle portion is presented in types of calcite infilling (Fig. 10). Since calcite crystals usually grow from pore walls, euhedral crystals surrounded by epitaxial crystals in the inner portion of tangential section (Figs. 7C, D) along with Type 1 surrounded by Type 2 or 3 and Type 2 surrounded by Type 3 in the radial section (Fig. 10) further imply that calcite growth in pore canals starts from the middle portion of eggshell based on the distribution of Type 1 to 3 which successively pushed sedimentary infills away to the external and internal eggshell surface. The displacement of sediment grains is a common phenomenon in crystal growth including calcite (Murray, 1964; Rees et al., 1976).

The main factor that decides epitaxial overgrowth is control of substrate that the overgrowing crystal is attached to (Dickson, 1993). Epitaxy happens when the substrate is active (crystals grow by seeding onto the substrate). In contrast, when the substrate is passive, crystals grow by nucleation on the substrate surface, and then euhedral crystals are made. Epitaxial overgrowth is known to have occurred in biogenic calcite and protein fibers (Aizenberg et al., 1994) and indeed has been observed in fossils of echinoderm (Dickson, 1993 and references therein), coral (Coronado et al., 2015), brachiopod (Casella et al., 2018), and eggshell (Choi et al., in press). Since the eggshell serves as a suitable system for protein preservation (Moreno-Azanza et al., 2016), epitaxial crystals in *P. widoensis* might have grown in the early stage of diagenesis when eggshell protein was preserved. However, on which condition epitaxial overgrowth initiates in the eggshell system is unknown and thereby, requires further studies.

Cathodoluminescence (Grellet-Tinner et al., 2010) and EBSD (Grellet-Tinner et al., 2011; Eagle et al., 2015) have been used to detect eggshell diagenesis in previous studies. However, as seen in Type 1 (Mn-deficient epitaxial crystal) of *P. widoensis*, CL and EBSD failed to identify calcite precipitated from Mn-free fluid and epitaxial crystals that are indistinguishable with neighboring shell units, respectively. Mg distribution map was the only method that could detect the presence of Type 1 calcite infill. Mg and Mn are representative and compatible elements in calcite and therefore, their composition in the carbonate rock shows a wide range of variation. As compatible element/Ca ratios of biogenic and diagenetic carbonates differ from each other, they function as a tool to detect diagenesis (Ullmann and Korte, 2015). Furthermore, the content of Mg incorporated in calcite overgrowth is mainly determined by the concentration of fluid that precipitates it (Mucci and Morse, 1983). Therefore, if overgrown calcite crystals are precipitated by fluid that has different Mg concentration, precipitated crystals can be identified by Mg distribution map. On the other hand, detecting epitaxial overgrowth is important in fossil eggshell study. Epitaxial overgrowth of eggshell has been reported in pore infilling (Grellet-Tinner et al., 2011; Moreno-Azanza et al., 2016) and on the external surface (Choi et al., in press). Especially, those presented on the external surface are important as it can be easily mistaken as a biological layer. Recently, Choi et al. (in press) have identified a diagenetic epitaxial layer on the external surface of *Prismatoolithus levis* by using BSE and Mg distribution map. The epitaxial portion was significantly deficient in Mg concentration than that of eggshell. Therefore, the difference of Mg incorporation in eggshell and diagenetic calcites including epitaxial crystal serve as powerful tools to identify diagenesis as well as the presence of Mn. In addition, elemental analysis combined with light microscopy, EBSD and CL effectively provide a detailed diagenetic history such as pore infilling and epitaxial overgrowth.

5.5. *Paleobiology of the* Propagoolithus *and faveoloolithid egg-layers*

About faveoloolithid egg-layers, a sauropod affinity was proposed due to skeletal remains of sauropods found in nearby the egg-bearing layer or similarity in nesting behavior to that of titanosaurs (Megaloolithidae), or the huge size of eggs (Faccio, 1994; Mikhailov, 1997a; Grellet-Tinner and Fiorelli, 2010). This hypothesis based on circumstantial or indirect evidence has been accepted and used in a number of articles (Paik et al., 2004; Fiorelli et al., 2012; Grellet-Tinner et al., 2012; García et al., 2015; Hechenleitner et al., 2016, 2018; Tanaka et al., 2018). However, since no single embryo fossil associated with faveoloolithid eggs was found, it is more reasonable to say that the egg-layers of Faveoloolithidae are unknown until direct skeletal evidence is found.

Despite the unclear taphonomic affinity, faveoloolithid eggs, often associated with clutches, are frequently found in the Cretaceous deposits of Northeast Asia and South America, giving insights into the nesting behavior (Mikhailov, 1997a and references therein; Huh and Zelenitsky, 2002; Grellet-Tinner and Fiorelli, 2010). Although complicated branching shell units and pore canals impede direct calculation of porosity, *P. widoensis* has an extremely large number of pore canals as in other faveoloolithid eggs. This indicates that *P. widoensis* was incubated in a covered nest or buried in a substrate (Deeming, 2006; Grellet-Tinner et al., 2012). The distribution of eggs and clutches of *P. widoensis* does not appear to be moved from their original positions. Recently, Tanaka et al. (2018) have claimed that the faveoloolithid egg-layers preferred in-filled hole nests using inorganic heat sources such as solar or geothermal energy to mound nest using an organic heat source based on the fact that the majority of them are found in coarse-grained deposits. However, unlike most of the faveoloolithid eggs, *P. widoensis* was found in fine-grained deposits, implying that progenitors of *P. widoensis* may have used organic heat source for their nests.

Clutches of eggs are observable in several different stratigraphic horizons in Wi Island egg site (Fig. 2). Nesting site fidelity is frequently observed in extant birds, reptiles, and mammals (Switzer, 1993) as well as in dinosaurs (Horner, 1982; Chiappe et al., 1998). However, interpreting occurrence of eggs as neontological site fidelity needs caution as the time interval between egg-bearing stratigraphic horizons is much longer than that of neontological site fidelity and should be interpreted in a geological time scale (Sander et al., 2008). Therefore, the term 'paleontological site fidelity' (*sensu* Varricchio et al., 2015), or repeated use of a nesting site in geologic time, is more appropriate to describe the repeated occurrence of clutches in Wi Island egg site. The colonial nesting ground which shows 'paleontological site fidelity' of the Faveoloolithidae was already reported from the Hwaseong and Boseong egg sites from South Korea (Lee, 2003; Paik et al., 2004; Kim et al., 2009) and the Sanagasta and Rio Negro sites from Argentina (Salgado et al., 2007; Grellet-Tinner and Fiorelli, 2010). Therefore, the Wi Island egg site provides another example of the egg-layering behavior of Faveoloolithidae, suggesting that the faveoloolithid egg-layers were colonial nesters and visited the same sedimentary environment repeatedly in geologic time.

6. Conclusions

Forty-one of the same type of dinosaur eggs were found from the Upper Cretaceous Wido Volcanics from Wi Island, South Korea. Clutches of eggs were found in seven different stratigraphic horizons, suggesting a colonial nesting ground and paleontological site fidelity. The slender shell units with numerous pore canals shown in the radial thin section confirm the assignment to Faveoloolithidae. However, shell units branch upward and pore canal width

accordingly becomes smaller towards the eggshell external surface. These characters support the erection of a new ootaxon, *Propagoolithus widoensis*. The crystallographic analyses using EBSD and three-dimensional reconstruction of eggshell provided new insights into the oofamily Faveoloolithidae: (1) Superimposed shell unit is a taphonomic artifact, thereby no use as a diagnosis and a major parataxonomic revision is needed for the Faveoloolithidae, Dictyoolithidae, and Similifaveoloolithidae, (2) Rounded shell units and their connections (bridges) separated by irregular pore canals in the lower portion of eggshell can be used as an additional synapomorphy of the Faveoloolithidae. Our study supports the view that elemental analysis coupled with light microscopy, EBSD, and CL is a powerful method to trace a detailed diagenetic history of eggshell such as pore infilling events. In addition, Mg can be served as a proxy for identifying epitaxial growth.

Acknowledgements

We thank Dr. I.G. Hwang in KIGAM (Korea Institute of Geoscience and Mineral Resources) who discovered and informed us the dinosaur eggs in Wi Island. J.-W Park (Marine Petrology and Geochemistry Laboratory, SNU) provided a polarization microscope and J.H. Kim assisted in taking images. We also thank S. Kim (National Center for Inter University Research Facilities, SNU) who helped us in using FE-EPMA. We debt to E.J. Park, H.W. Lee (Paleontological Laboratory, SNU), and S.H. Kim for their assistance in the field. E.J. Park provided aerial photographs of the study area. We are grateful to an anonymous reviewer and to Dr. D.E. Barta for their critical and constructive comments on our earlier version of the manuscript. This research was supported by National Research Foundation of Korea (grant number: 2016R1A2B2015012) to the corresponding author.

References

Aizenberg, J., Albeck, S., Weiner, S., Addadi, L., 1994. Crystal-protein interactions studied by overgrowth of calcite on biogenic skeletal elements. Journal of Crystal Growth 142, 156–164.

Araújo, R., Castanhinha, R., Martins, R.M.S., Mateus, O., Hendrickx, C., Beckmann, F., Schell, N., Alves, L.C., 2013. Filling the gaps of dinosaur eggshell phylogeny: Late Jurassic theropod clutch with embryos from Portugal. Scientific Reports 3, 1924.

Barnaby, R.J., Rimstidt, J.D., 1989. Redox conditions of calcite cementation interpreted from Mn and Fe contents of authigenic calcites. Geological Society of America Bulletin 101, 795–804.

Barta, D.E., Brundridge, K.M., Croghan, J.A., Jackson, F.D., Varricchio, D.J., Jin, X., Poust, A.W., 2014. Eggs and clutches of the Spheroolithidae from the Cretaceous Tiantai basin, Zhejiang Province, China. Historical Biology 26, 183–194.

Blair, T.C., McPherson, J.G., 2009. Processes and forms of alluvial fans. In: Parsons, A.J., Abrahams, A.D. (Eds.), Geomorphology of Desert Environments, second ed. Springer, Dordrecht, pp. 413–467.

Bull, W.B., 1977. The alluvial-fan environment. Progress in Physical Geography 1, 222–270.

Casella, L.A., Griesshaber, E., Simonet Roda, M., Ziegler, A., Mavromatis, V., Henkel, D., Laudien, J., Häussermann, V., Neuser, R.D., Angiolini, L., Dietzel, M., Eisenhauer, A., Immenhauser, A., Brand, U., Schmahl, W.W., 2018. Micro-and nanostructures reflect the degree of diagenetic alteration in modern and fossil brachiopod shell calcite: A multi-analytical screening approach (CL, FE-SEM, AFM, EBSD). Palaeogeography, Palaeoclimatology, Palaeoecology 502, 13–30.

Chiappe, L.M., Coria, R.A., Dingus, L., Jackson, F., Chinsamy, A., Fox, M., 1998. Sauropod dinosaur embryos from the Late Cretaceous of Patagonia. Nature 396, 258–261.

Choi, S., Han, S., Kim, N.-H., Lee, Y.-N., 2018. A comparative study of eggshells of Gekkota with morphological, chemical compositional and crystallographic approaches and its evolutionary implications. PLoS ONE 13, e0199496.

Choi, S., Han, S., Lee, Y.-N., 2019. Electron Backscatter Diffraction (EBSD) analysis of maniraptoran eggshells with important implications for microstructural and taphonomic interpretations. Palaeontology (in press).

Chough, S.K., 2013. Geology and Sedimentology of the Korean Peninsula. Elsevier, Amsterdam.

Chough, S.K., Kwon, S.-T., Ree, J.-H., Choi, D.K., 2000. Tectonic and sedimentary evolution of the Korean peninsula: a review and new view. Earth-Science Reviews 52, 175–235.

Chun, S.S., Chough, S.K., 1992. Tectonic history of Cretaceous sedimentary basins in the southwestern Korean Peninsula and Yellow Sea. In: Chough, S.K. (Ed.), Sedimentary Basins in the Korean Peninsula and Adjacent Seas. Korean Sedimentary Research Group Special Publication, Harnlimwon Publishers, Seoul, pp. 60–76.

Clayburn, J.K., Smith, D.L., Hayward, J.L., 2004. Taphonomic effects of pH and temperature on extant avian dinosaur eggshell. Palaios 19, 170–177.

Coronado, I., Fernández-Martínez, E., Rodríguez, S., Tourneur, F., 2015. Reconstructing a Carboniferous inferred coral–alcyonarian association using a biomineralogical approach. Geobiology 13, 340–356.

Cree, A., Guillette Jr., L.J., Reader, K., 1996. Eggshell formation during prolonged gravidity of the tuatara *Sphenodon punctatus*. Journal of Morphology 230, 129–144.

Dalbeck, P., Cusack, M., 2006. Crystallography (electron backscatter diffraction) and chemistry (electron probe microanalysis) of the avian eggshell. Crystal Growth & Design 6, 2558–2562.

Dauphin, Y., Luquet, G., Perez-Huerta, A., Salomé, M., 2018. Biomineralization in modern avian calcified eggshells: similarity versus diversity. Connective Tissue Research 58, 67–73.

Deeming, D.C., 2006. Ultrastructural and functional morphology of eggshells supports the idea that dinosaur eggs were incubated buried in a substrate. Palaeontology 49, 171–185.

Dickson, J.A.D., 1993. Crystal growth diagrams as an aid to interpreting the fabrics of calcite aggregates. Journal of Sedimentary Petrology 63, 1–17.

Dromgoole, E.L., Walter, L.M., 1990. Iron and manganese incorporation into calcite: Effects of growth kinetics, temperature and solution chemistry. Chemical Geology 81, 311–336.

Eagle, R.A., Enriquez, M., Grellet-Tinner, G., Pérez-Huerta, A., Hu, D., Tütken, T., Montanari, S., Loyd, S.J., Ramirez, P., Tripati, A.K., Kohn, M.J., Cerling, T.E., Chiappe, L.M., Eiler, J.M., 2015. Isotopic ordering in eggshells reflects body temperatures and suggests differing thermophysiology in two Cretaceous dinosaurs. Nature Communications 6, 8296.

Faccio, G., 1994. Dinosaurian eggs from the Upper Cretaceous of Uruguay. In: Carpenter, K., Hirsch, K.F., Horner, J.R. (Eds.), Dinosaur Eggs and Babies. Cambridge University Press, New York, pp. 47–55.

Fang, X., Lu, L., Cheng, Z., Zou, Y., Pang, Q., Wang, Y., Chen, K., Yin, Z., Wang, X., Liu, J., Xie, H., Jin, Y., 1998. On the Cretaceous Fossil Eggs of Xixia County, Henan Province. Geological Publishing House, Beijing.

Ferrill, D.A., Morris, A.P., Evans, M.A., Burkhard, M., Groshong Jr., R.H., Onasch, C.M., 2004. Calcite twin morphology: a low-temperature deformation geothermometer. Journal of Structural Geology 26, 1521–1529.

Fiorelli, L.E., Grellet-Tinner, G., Alasino, P.H., Argañaraz, E., 2012. The geology and palaeoecology of the newly discovered Cretaceous neosauropod hydrothermal nesting site in Sanagasta (Los Llanos Formation), La Rioja, northwest Argentina. Cretaceous Research 35, 94–117.

García, R.A., Salgado, L., Fernández, M.S., Cerda, I.A., Paulina-Carabajal, A., Otero, A., Coria, R.A., Fiorelli, L.E., 2015. Paleobiology of titanosaurs: reproduction, development, histology, pneumaticity, locomotion and neuroanatomy from the South American fossil record. Ameghiniana 52, 29–68.

Gihm, Y.S., Hwang, I.G., 2014. Syneruptive and intereruptive lithofacies in lacustrine environments: the Cretaceous Beolkeum Member, Wido Island, Korea. Journal of Volcanology and Geothermal Research 273, 15–32.

Gihm, Y.S., Kim, M.C., Son, M., Hwang, I.G., 2017. The influence of tectonic subsidence on volcaniclastic sedimentation: The Cretaceous upper Daeri Member, Wido Island, Korea. Island Arc 26 e12183.

Graf, J., Tabor, N.J., Ferguson, K., Winkler, D.A., Lee, Y.-N., May, S., Jacobs, L.L., 2018. Diagenesis of dinosaur eggshell from the Gobi Desert, Mongolia. Palaeogeography, Palaeoclimatology, Palaeoecology 494, 65–74.

Grellet-Tinner, G., 2005. Membrana testacea of titanosaurid dinosaur eggs from Auca Mahuevo (Argentina): implications for exceptional preservation of soft tissue in Lagerstätten. Journal of Vertebrate Paleontology 25, 99–106.

Grellet-Tinner, G., Fiorelli, L.E., 2010. A new Argentinean nesting site showing neosauropod dinosaur reproduction in a Cretaceous hydrothermal environment. Nature Communications 1, 32.

Grellet-Tinner, G., Chiappe, L.M., Coria, R., 2004. Eggs of titanosaurid sauropods from the Upper Cretaceous of Auca Mahuevo (Argentina). Canadian Journal of Earth Sciences 41, 949–960.

Grellet-Tinner, G., Corsetti, F., Buscalioni, A.D., 2010. The importance of microscopic examinations of eggshells: Discrimination of bioalteration and diagenetic overprints from biological features. Journal of Iberian Geology 36, 181–192.

Grellet-Tinner, G., Sim, C.M., Kim, D.H., Trimby, P., Higa, A., An, S.L., Oh, H.S., Kim, T., Kardjilov, N., 2011. Description of the first lithostrotian titanosaur embryo *in ovo* with Neutron characterization and implications for lithostrotian Aptian migration and dispersion. Gondwana Research 20, 621–629.

Grellet-Tinner, G., Fiorelli, L.E., Salvador, R.B., 2012. Water vapor conductance of the Lower Cretaceous dinosaurian eggs from Sanagasta, La Rioja, Argentina: paleobiological and paleoecological implications for South American faveoloolithid and megaloolithid eggs. Palaios 27, 35–47.

Groshong Jr., R.H., 1972. Strain calculated from twinning in calcite. Geological Society of America Bulletin 83, 2025–2038.

He, Q., Zhang, S., Xing, L., Jiang, Q., Wang, X., Pan, Z., Hu, Y., 2017. A new oospecies of Similifaveoloolithidae from the Xiuning Basin, Late Cretaceous of Anhui, China. Historical Biology. https://doi.org/10.1080/08912963.2017.1351440.

Hechenleitner, E.M., Grellet-Tinner, G., Foley, M., Fiorelli, L.E., Thompson, M.B., 2016. Micro-CT scan reveals an unexpected high-volume and interconnected pore network in a Cretaceous Sanagasta dinosaur eggshell. Journal of the Royal Society Interface 13, 20160008.

Hechenleitner, E.M., Taborda, J.R.A., Fiorelli, L.E., Grellet-Tinner, G., Nuñez-Campero, S.R., 2018. Biomechanical evidence suggests extensive eggshell thinning during incubation in the Sanagasta titanosaur dinosaurs. PeerJ 6, e4971.
Horner, J.R., 1982. Evidence of colonial nesting and 'site fidelity' among ornithischian dinosaurs. Nature 297, 675–676.
Huh, M., Zelenitsky, D.K., 2002. Rich dinosaur nesting site from the Cretaceous of Bosung County, Chullanam-do Province, South Korea. Journal of Vertebrate Paleontology 22, 716–718.
Jackson, F.D., Schmitt, J.G., 2008. Recognition of vertebrate egg abnormalities in the Upper Cretaceous fossil record. Cretaceous Research 29, 27–39.
Jin, X., Jackson, F.D., Varricchio, D.J., Azuma, Y., He, T., 2010. The first *Dictyoolithus* egg clutches from the Lishui Basin, Zhejiang Province, China. Journal of Vertebrate Paleontology 30, 188–195.
Kim, J.Y., Yang, S.Y., Choi, H.I., Seo, S.J., Kim, K.S., 2011. Dinosaur eggs from the Cretaceous Goseong Formation of Tongyeong City, southern coast of Korea. Journal of the Paleontological Society of Korea 27, 13–26.
Kim, S.B., Kim, Y.-G., Jo, H.R., Jeong, K.S., Chough, S.K., 2009. Depositional facies, architecture and environments of the Sihwa Formation (Lower Cretaceous), mid-west Korea with special reference to dinosaur eggs. Cretaceous Research 30, 100–126.
Ko, K., Kim, S.W., Lee, H.-J., Hwang, I.G., Kim, B.C., Kee, W.-S., Kim, Y.-S., Gihm, Y.S., 2017. Soft sediment deformation structures in a lacustrine sedimentary succession induced by volcano-tectonic activities: An example from the Cretaceous Beolgeumri Formation, Wido Volcanics, Korea. Sedimentary Geology 358, 197–209.
Koh, H.J., Kwon, C.W., Park, S.I., Park, J., Kee, W.S., 2013. Geological report of the Julpo and Wido-Hawangdeungdo sheets (1: 50,000). Korea Institute of Geoscience and Mineral Resources, p. 81 (in Korean with English abstract).
Lee, Y.-N., 2003. Dinosaur bones and eggs in South Korea. Memoir of the Fukui Prefectural Dinosaur Museum 2, 113–121.
Liu, J.-Y., Zhao, Z.-K., 2004. A new oospecies of the dinosaur eggs (*Dictyoolithus*) from Laiyang, Shandong Province. Vertebrata PalAsiatica 42, 166–170.
Mikhailov, K.E., 1994. Eggs of sauropod and ornithopod dinosaurs from the Cretaceous deposits of Mongolia. Paleontological Journal 28, 141–159.
Mikhailov, K.E., 1997a. Fossil and recent eggshell in amniotic vertebrates: fine structure, comparative morphology and classification. Special Papers in Palaeontology 56, 1–80.
Mikhailov, K.E., 1997b. Avian eggshells: an atlas of scanning electron micrographs. British Ornithologists' Club Occasional Publications 3, 1–88.
Moreno-Azanza, M., Mariani, E., Bauluz, B., Canudo, J.I., 2013. Growth mechanisms in dinosaur eggshells: an insight from electron backscatter diffraction. Journal of Vertebrate Paleontology 33, 121–130.
Moreno-Azanza, M., Bauluz, B., Canudo, J.I., Gasca, J.M., Fernández-Baldor, F.T., 2016. Combined use of electron and light microscopy techniques reveals false secondary shell units in Megaloolithidae eggshells. PLoS ONE 11, e0153026.
Moreno-Azanza, M., Bauluz, B., Canudo, J.I., Mateus, O., 2017. The conservative structure of the ornithopod eggshell: electron backscatter diffraction characterization of *Guegoolithus turolensis* from the Early Cretaceous of Spain. Journal of Iberian Geology 43, 235–243.
Mucci, A., Morse, J.W., 1983. The incorporation of Mg^{2+} and Sr^{2+} into calcite overgrowths: influences of growth rate and solution composition. Geochimica et Cosmochimica Acta 47, 217–233.
Murray, R.C., 1964. Origin and diagenesis of gypsum and anhydrite. Journal of Sedimentary Research 34, 512–523.
Nadon, G.C., Issler, D.R., 1997. The compaction of floodplain sediments: timing, magnitude and implications. Geoscience Canada 24, 37–43.
Packard, M.J., Thompson, M.B., Goldie, K.N., Vos, M., 1988. Aspects of shell formation in eggs of the tuatara, *Sphenodon punctatus*. Journal of Morphology 197, 147–157.
Pagel, M., Barbin, V., Blanc, P., Ohnenstetter, D., 2000. Cathodoluminescence in Geosciences: An Introduction. In: Pagel, M., Barbin, V., Blanc, P., Ohnenstetter, D. (Eds.), Cathodoluminescence in Geosciences. Springer, Berlin, pp. 1–21.
Paik, I.S., Huh, M., Kim, H.J., 2004. Dinosaur egg-bearing deposits (Upper Cretaceous) of Boseong, Korea: occurrence, palaeoenvironments, taphonomy, and preservation. Palaeogeography, Palaeoclimatology, Palaeoecology 205, 155–168.
Pérez-Huerta, A., Dauphin, Y., 2016. Comparison of the structure, crystallography and composition of eggshells of the guinea fowl and graylag goose. Zoology 119, 52–63.
Pingitore Jr., N.E., Eastman, M.P., Sandidge, M., Oden, K., Freiha, B., 1988. The coprecipitation of manganese (II) with calcite: an experimental study. Marine Chemistry 25, 107–120.
Prior, D., 1999. Problems in determining the misorientation axes, for small angular misorientations, using electron backscatter diffraction in the SEM. Journal of Microscopy 195, 217–225.
Rees, M.N., Brady, M.J., Rowell, A.J., 1976. Depositional environments of the Upper Cambrian Johns Wash Limestone (House Range, Utah). Journal of Sedimentary Petrology 46, 38–47.
Salgado, L., Coria, R.A., Ribeiro, C.M.M., Garrido, A., Rogers, R., Simón, M.E., Arcucci, A.B., Rogers, K.C., Paulina-Carabajal, A., Apesteguía, S., Fernández, M., García, R.A., Talevi, M., 2007. Upper Cretaceous dinosaur nesting sites of Río Negro (Salitral Ojo de Agua and Salinas de Trapalcó-Salitral de Santa Rosa), northern Patagonia, Argentina. Cretaceous Research 28, 392–404.
Sander, P.M., Petiz, C., Jackson, F.D., Chiappe, L.M., 2008. Upper Cretaceous titanosaur nesting sites and their implications for sauropod dinosaur reproductive biology. Palaeontolgraphica Abteilung A 284, 69–107.
Schmidt, W.J., 1962. Liegt der Eischalenkalk der Vögel als submikroskopische Kristallite vor? Zeitschrift für Zellforschung und Mikroskopische Anatomie 57, 848–880 (in German).
Sharma, N.K., Shekhar, S., 2018. Deconvoluting error in measurement of low angle misorientation distribution. Micron 107, 28–34.
Switzer, P.V., 1993. Site fidelity in predictable and unpredictable habitats. Evolutionary Ecology 7, 533–555.
Tanaka, K., Zelenitsky, D.K., Therrien, F., Kobayashi, Y., 2018. Nest substrate reflects incubation style in extant archosaurs with implications for dinosaur nesting habits. Scientific Reports 8, 3170.
Tyler, C., Moore, D., 1965. Types of damage caused by various cracking and crushing methods used for measuring egg shell strength. British Poultry Science 6, 175–182.
Ullmann, C.V., Korte, C., 2015. Diagenetic alteration in low-Mg calcite from macrofossils: a review. Geological Quarterly 59, 3–20.
Varricchio, D.J., Jackson, F.D., 2004. A phylogenetic assessment of prismatic dinosaur eggs from the Cretaceous Two Medicine Formation of Montana. Journal of Vertebrate Paleontology 24, 931–937.
Varricchio, D.J., Jin, X., Jackson, F.D., 2015. Lay, brood, repeat: nest reuse and site fidelity in ecologic time for two Cretaceous troodontid dinosaurs. Journal of Vertebrate Paleontology 35, e932797. https://doi.org/10.1080/02724634.2014.932797.
Vianey-Liaud, M., Jain, S.L., Sahni, A., 1987. Dinosaur eggshells (Saurischia) from the Late Cretaceous intertrappean and Lameta Formations (Deccan, India). Journal of Vertebrate Paleontology 7, 408–424.
Vila, B., Jackson, F.D., Fortuny, J., Sellés, A.G., Galobart, À., 2010. 3-D modelling of megaloolithid clutches: insights about nest construction and dinosaur behaviour. PLoS ONE 5, e10362.
Wang, Q., Zhao, Z.-K., Wang, X.-L., Jiang, Y.-G., 2011. New ootypes of dinosaur eggs from the Late Cretaceous in Tiantai Basin, Zhejiang Province, China. Vertebrata PalAsiatica 49, 446–449.
Wang, Q., Zhao, Z., Wang, X., Zhang, S., Jiang, Y., 2013. New forms of dictyoolithids from the Tiantai Basin, Zhejiang Province of China and a parataxonomic revision of the dictyoolithids. Vertebrata PalAsiatica 51, 43–54.
Wang, X.-l., Wang, Q., Jiang, S.-x., Cheng, X., Zhang, J.-l., Zhao, Z.-k., Jiang, Y.-g., 2012. Dinosaur egg faunas of the Upper Cretaceous terrestrial red beds of China and their stratigraphical significance. Journal of Stratigraphy 36, 400–416.
Wheeler, J., Prior, D.J., Jiang, Z., Spiess, R., Trimby, P.W., 2001. The petrological significance of misorientations between grains. Contributions to Mineralogy and Petrology 141, 109–124.
Wilson, H.M., Heck, C.T., Varricchio, D.J., Jackson, F.D., Jin, X., 2014. Evaluating deformation in *Spheroolithus* dinosaur eggs from Zhejiang, China. Historical Biology 26, 173–182.
Wilson, M.E.J., Evans, M.J., 2002. Sedimentology and diagenesis of Tertiary carbonates on the Mangkalihat Peninsula, Borneo: implications for subsurface reservoir quality. Marine and Petroleum Geology 19, 873–900.
Zhang, S.-K., 2010. A parataxonomic revision of the Cretaceous faveoloolithid eggs of China. Vertebrata PalAsiatica 48, 203–219 (in Chinese with English summary).
Zhang, S., Yang, T.-R., Li, Z., Hu, Y., 2018. New dinosaur egg material from Yunxian, Hubei Province, China resolves the classification of dendroolithid eggs. Acta Palaeontologica Polonica 63, 671–678.
Zhao, Z.-K., 1979a. Discovery of the dinosaurian eggs and footprint from Neixiang County, Henan Province. Vertebrata PalAsiatica 17, 304–309 (in Chinese with English abstract).
Zhao, Z.-K., 1979b. Progress in the Research of Dinosaur Eggs. In: Institute of Vertebrate Paleontology and Paleoanthropology, Nanjing Institute of Paleontology (Eds.), Mesozoic and Cenozoic Red Beds of South China. Science Press, Beijing, pp. 330–340.
Zhao, Z.-K., 1994. Dinosaur eggs in China: on the structure and evolution of eggshells. In: Carpenter, K., Hirsch, K.F., Horner, J.R. (Eds.), Dinosaur Eggs and Babies. Cambridge University Press, New York, pp. 184–203.
Zhao, Z.-K., Ding, S.R., 1976. Discovery of the dinosaur eggs from Alashanzuoqi and its stratigraphical meaning. Vertebrata PalAsiatica 14, 42–45 (in Chinese).
Zou, S.L., Wang, Q., Wang, X.-L., 2013. A new oospecies of parafaveoloolithids from the Pingxiang Basin, Jiangxi Province of China. Vertebrata PalAsiatica 51, 102–106 (in Chinese with English abstract).

Appendix A. Supplementary data

Supplementary data to this article can be found online at https://doi.org/10.1016/j.cretres.2019.04.001.